P-11-20

Äspö Hard Rock Laboratory

Sorption experiments and leaching studies using fault gouge and rim zone material from the Äspö Hard Rock Laboratory

TRUE-1 Continuation project

Johan Byegård, Geosigma AB

Eva-Lena Tullborg, Terralogica AB

Juni 2012

Svensk Kärnbränslehantering AB
Swedish Nuclear Fuel
and Waste Management Co

Box 250, SE-101 24 Stockholm
Phone +46 8 459 84 00

ISSN 1651-4416
SKB P-11-20
ID 1378492

Äspö Hard Rock Laboratory

Sorption experiments and leaching studies using fault gouge and rim zone material from the Äspö Hard Rock Laboratory

TRUE-1 Continuation project

Johan Byegård, Geosigma AB

Eva-Lena Tullborg, Terralogica AB

Juni 2012

Keywords: Fault gouge, Fracture, Laboratory, Leaching, Modelling, Rim zone, Sorption.

Abstract

A series of sorption studies have been performed in which sorption properties of fault gouge material and rim zone material have been determined, mainly by batch sorption experiment technique. The study focused on the part of the Äspö Hard Rock Laboratory (Oskarshamn, Sweden) where the TRUE Block Scale Experiments (*in situ* tracer test using sorbing tracers) have been performed. One major aim of the current experiments was thus to obtain site specific retention properties to use in the interpretation, but the investigations were also focused on obtaining general sorption properties of different types of fault gouge materials. The tracers involved in the study were mainly radiotracers that were assumed to sorb by a cation exchange mechanism, i.e. $^{22}Na^{+}$, $^{45}Ca^{2+}$, $^{86}Rb^{+}$, $^{85}Sr^{2+}$, $^{137}Cs^{+}$, $^{133}Ba^{2+}$ and $^{226}Ra^{2+}$. Besides these elements, the $^{54}Mn^{2+}$ (assumed to also be influenced by surface complexation) tracer was included in the study.

The results indicated a strong heterogeneity especially for the different fault gouge materials. There was a variation in the sorption capacity (demonstrated by the results of the cation exchange capacity as well as the BET specific surface area) and also a variation in the selectivity between the different cations was observed. For example, the gouge materials containing different clay minerals showed high sorption coefficients (K_d) for e.g. Rb^{+} and Cs^{+} while the materials containing different forms of iron oxides showed high sorption for the Mn^{2+} tracer which is expected to be influenced by surface complexation sorption.

Sorption studies using the rim zone material (in this case, crystalline rock material with different degrees of alteration, located closest to the water conducting fractures) also showed a varying sorption. It is shown that the sorption coefficients for materials sampled within an interpreted single geological structure within a block scale can vary up to a factor of ten.

Modelling of the batch sorption results indicated difficulties in the interpretation of the time dependence of the sorption using a matrix diffusion model. The implications of the size fractions chosen for the batch sorption technique were discussed.

In this work, a study is also included where the different techniques of leaching and cation exchange capacity were compared. The relatively new method of cation exchange capacity determination comprising a saturation with cobalt hexamine, $Co(III)(NH_3)_6^{3+}$, was tested and shown to be promising. An attempt was also made to perform a complexing agent leaching (EDTA) of tracer elements from the rock material and comparing this to the natural water concentration of these tracers; i.e. a possible alternative technique for sorption coefficient determination.

Contents

1 Introduction

For the interpretation of the results of tracer experiments done within the framework of the Tracer Retention Understanding Experiment (TRUE), the interaction of the tracers with the fault gouge material and rim zone material has been considered an important process (e.g. Winberg et al. 2000, Poteri et al. 2002). Laboratory investigations of the retention characteristics of geological materials from the Äspö Hard Rock Laboratory (ÄHRL) have earlier been done on rim zone material from Feature A at the TRUE site (Byegård et al. 1998, 2001). Because of the difficulties in isolating the unconsolidated fault gouge material during drilling, only small quantities of fault gouge material have been recovered for the fractures associated with the hydraulic structures involved in the TRUE program.

No sorption studies have therefore so far been performed using fault gouge material. For modelling of the results from the TRUE Block Scale Experiment (TRUE BS), estimations of sorption coefficients (K_d) were made using the mineralogy for the fault gouge material combined with literature data for the cation exchange capacity of the pure mineral phases. However, a need has been identified of actual experimental results of the sorption characteristics of fault gouge material; both for the interpretation of the results of *in situ* experiments and also for performance assessment (PA) applications, e.g. the on-going SKB site investigation program.

Furthermore, the drillings for the Fault Rock Zone characterization program (Hakami and Wang 2005) yielded significant amounts of fault gouge material from features that resemble the mylonitic zones that were experimented upon in the TRUE-1 and TRUE Block Scale tracer experiments. This observation, together with the finding of fault gouge material in zone EW-1, zone NE-1 and in zone Z (Andersson et al. 2002a) has therefore been a motivation for initiation of a general project studying the sorption characteristics of fault gouge materials, exemplified with materials from the ÄHRL.

It has also been identified that the amount of sorption data addressing the interaction in the rim zone of water conducting fractures mainly originates from the TRUE-1 laboratory experiments, e.g. Byegård et al. (1998, 2001). However, in the TRUE Block Scale tracer experiments (Andersson et al. 2002a, b), transport studies were related to flow paths involving several different fracture types of different complexity. For the interpretation of these tests and also of other tracer experiments performed in the block scale (Andersson et al. 2007) it can be foreseen that a larger basis for the data describing the interaction in the facture rim zones could provide a better basis for understanding the retention observed in *in situ* tracer experiments.

An attempt to semi-deterministically make use of the results of the fracture observations in the TRUE Block Scale experiment was done as part of the Äspö Task Force (Task 6) (Dershowitz et al. 2003) where these data were applied to a performance assessment calculation. One can therefore also foresee that a larger basis of fracture retention properties would be useful for different performance assessment applications, e.g. for the on-going SKB site investigation program.

The main objectives of this study can therefore be summarized as:

- Provide sorption data for the interaction of this material with the type of sorbing tracers so far used in the TRUE program. This group consists mainly of tracers sorbing with cation exchange as the major mechanism, e.g. Na^+, Ca^{2+}, Rb^+, Sr^{2+}, Cs^+ and Ba^{2+}. Furthermore, the tracer Mn^{2+} (with its sorption assumed be influenced by surface complexation), showed pronounced retardation, yet with high recovery in the TRUE Block Scale Continuation Experiment (Andersson et al. 2007) and was therefore also included in this experiment.
- Make sorption studies using geologic material from Structure #13, Structure #19, Structure #20 and Structure #22 in the TRUE Block Scale rock block. Structures #13, #20 and #22 are interpreted to have been involved in the different flow paths in the TRUE Block Scale phase C experiment. Structure #19 was the major target for the TRUE Block Scale Continuation experiment (Andersson et al. 2007).
- Make sorption studies addressing fault gouge material from the SKB site investigation. This activity is meant to act as a link between the TRUE and the laboratory sorption experiments program of the site investigation program (Widestrand et al. 2003).

Furthermore, some additional complementary experimental investigations were performed with the following objectives:

- Provide the cation exchange characteristics of the materials, i.e. estimation of the cation exchange capacity, the fractional occupancies and the selectivity coefficients. This is performed in order to evaluate the validity of the predictions of sorption properties of fault gouge materials made by Andersson et al. (2002a).
- Perform desorption experiments with varying strength of desorption agents (different concentrations of the cation exchange competitor ammonium acetate, different concentrations of the complexing agent EDTA). This will be performed as a test to evaluate the sorption strength of naturally occurring cationic tracers (e.g. lanthanides, thorium and uranium) and, possibly, to form the basis for *in situ* sorption experiment.
- A test of the possibility of determining sorption coefficients using low levels of α-emitting isotopes (Am-241 and Ra-226, as proposed in the laboratory experiment strategy document for the SKB Site Investigation Program, Widestrand et al. 2003).

2 Experimental work

2.1 Material

For this investigation, two major types of rock material are used, fault gouge material and rim zone material.

2.1.1 Fault gouge material

Fault gouge material is non-consolidated materials that have been extracted from fractures without any crushing of the rock material. All materials used have been extracted from factures observed in drill cores; except for the 1596 m (NE-2) sample which has been excavated from the tunnel intercept with the NE-2 zone at tunnel length 1596 m. The extracted geological material was sieved, the <0.125 mm fraction used for the sorption experiment. For obtaining a logical and useful connection to the sorption investigations within the SKB site investigation program, a gouge material sampled at the very early stage of the Laxemar-Simpevarp site investigation was also included in the current work, sampled at the KSH02 borehole at 743 m borehole length.

A mineralogical description of the different materials used and results of the BET surface area measurements are given in Table 2-1. The chemical compositions of the material are given in Appendix A.

Table 2.1. Description of the fault gouge material used in the investigation.

Borehole or tunnel reference	Borehole length (m)	Zone (or TRUE BS structure #)	Mineralogic content	BET surface measurements (m^2/g)
Äspö material				
1303 m	n.a.	NE-1	Quartz, Potassium feldspar, Mixed Layer Clay, Chlorite, Illite	Not measured
1596 m	n.a.	NE-2	Chlorite, Corrensite, Quartz, Potassium feldspar, Calcite	3.47±0.07
2169 m	n.a		Quartz, Plagioclase, Potassium feldspar, Chlorite, Corrensite	1.61
KAS04	65	EW-1	Potassium feldspar, Chlorite, Illite, Mixed Layer Clay, Kaolinite	8.81
KI0025F	194	Z	Quartz, Potassium feldspar, Plagioclase, Chlorite, Illite	1.72
KI0025F02	133	#19	Chlorite, Smectite, Quartz, Plagioclase, Epidote, Illite	Not measured
KI0023B	69.9	#20	Chlorite, Illite, Calcite, Quartz, Potassium feldspar, Plagioclase, (Mixed Layer Clay)	Not measured
KI0025F02	66.7	#22	Chlorite, Mixed Layer Clay, Quartz, Potassium feldspar, Plagioclase, Calcite	Not measured
Simpevarp investigation area				
KSH02 borehole	743 m		Quartz, Potassium feldspar, Hematite, Chlorite, Plagioclase, Corrensite	10.05

2.1.2 Rim zone material

The rim zone materials used were sampled from fracture intercepts in cores obtained within the TRUE Block Scale Experiment program (Hermansson and Doe 2000). From the cores, a 0.5–1 cm thick slice parallel with the fracture plane was extracted (cf. Figure 2-1 for sample treatment). This slice was subsequently crushed and sieved to different size fractions. A thin section sample perpendicular to the fracture plane was also sampled.

From the different size fractions obtained, the 1–2 mm, 0.25–0.5 mm and <0.125 mm were used for the sorption experiments.

Photographs of the rim zone rock samples are given in Table 2-2 and a summary of the mineralogical composition (as determined from thin section analysis) are given in Table 2-3.

The rim zone material consists of altered quartz monzodiorite, with various amounts of mylonites. Cataclastic deformation (fragmentation of the rock and sealing with different secondary minerals) is common. The plagioclase is almost completely altered to albite, sericite and epidote (saussiritisation). Biotite is altered to chlorite and K feldspar has formed and used the excess potassium from the biotite breakdown. The feldspars are usually pigmented with micrograins of hematite which gives the red color, but the amounts of hematite are very small. Instead, magnetite and partly pyrite are the main opaque minerals (usually <1%). The rim zone is generally inhomogeneous both mineralogically and texturally and it is very difficult to give a modal composition. It can, however, be concluded that altered plagioclase (mainly albite) , quartz, epidote, chlorite and in K-feldspar makes up >95% of the wall rock and in the thin sections studied altered plagioclase makes up 40–60 vol% as an estimate. Point counting has not been possible due to very small grain sizes (and partly very small thin sections as well)

Additional minerals are e.g. sericite, calcite, magnetite, pyrite, fluorite, titanite and clay minerals like corrensite.

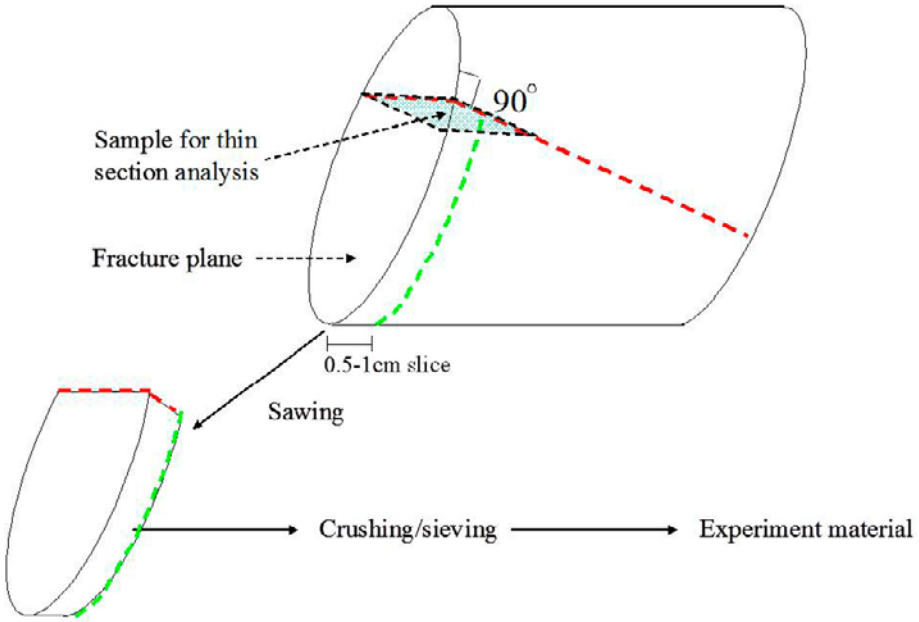

Figure 2-1. *Principle drawing of the extraction of rim zone material from the drill cores.*

Table 2-2. Photographs, location and geological descriptions of the rim zone rock material used in the investigation. The photographs refer to the fracture surface before sawing (left), the profile perpendicular to the fracture surface (middle) and the opposite side of the fracture obtained after the sawing of the sample (right).

KI0023B, 86.6 m, Structure #13 — Strongly tectonised and mylonitised rock type



KI0023B, 111.6 m Structure #19 — Mylonitic and cataclasitic wall rock, in Äspö diorite



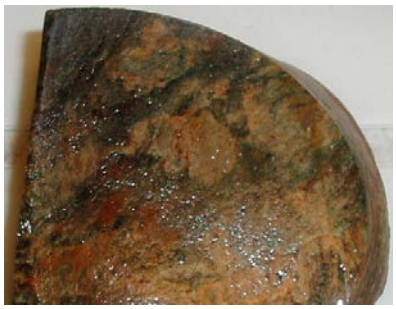

KI0025F, 166.65 m Structure #19 — Strongly hydrothermally altered rock



Table 2-2. Continued.

KI0023B, 69.9 m Structure #20

Strongly altered wall rock, representing an intermediate between cataclasite and mylonite



KI0025F02, 74,6 m Structure #20

Very thin mylonite closest to the fracture, altered granitoid



KI0025F02, 66.7m Structure #22

Strongly hydrothermally altered rock. Fault gouge material sampled in the same intercept contains mixed layer clay with high Cs+ concentrations



Table 2-3. Mineralogical compositions evaluated from thin section analyses, combined with the results from measurements of the BET surface area of the crushed and sieved samples of the different rim zone rock samples.

Sample ID and name of associated interpreted geological structure	Rock description	Mineralogical composition (thin section analyses)	BET surface area	
			Size fraction (mm)	Result (m^2/g)
KI0023B, 86.6 m Structure #13	Strongly tectonised and mylonitised rock type	Altered plagioclase, quartz, epidote, chlorite, K-feldspar, fluorite, opaque	N/A	
KI0023B, 111.6 m Structure #19	Mylonitic and cataclasitic wall rock, in Äspö diorite	Altered plagioclase, quartz, epidote, chlorite, K-feldspar, opaque, fluorite	<0.125 0.25–0.5 1–2	0.77 0.050 0.015
KI0025F, 166.65 m Structure #19	Strongly hydrothermally altered rock.	Altered plagioclase, chlorite, epidote, quartz, K-feldspar, fluorite, opaque, possible small remnants of altered biotite.	<0.125 0.25–0.5 1–2	2.68 1.59 0.86
KI0023B, 69.9 m Structure #20	Strongly altered wall rock, representing an intermediate between cataclasite and mylonite	Altered plagioclase, quartz, epidote, chlorite, K-feldspar, opaque	N/A	
KI0025F02, 74.,6 m Structure #20	Very thin mylonite closest to the fracture, altered granitoid	Altered plagioclase, quartz, epidote, chlorite, K-feldspar, opaque	N/A	
KI0025F02, 66.7 m Structure #22	Strongly hydrothermally altered rock	Altered plagioclase, quartz, chlorite, epidote, K-feldspar, opaque, clay minerals	N/A	

2.2 Laboratory experiment

In the experiment, all contact between water and rock material was performed in a nitrogen fed glovebox. Before the nitrogen was introduced in to the glovebox, the gas was purified from oxygen impurities in the nitrogen gas using a catalyst-based purifier.

2.2.1 Water phases

Synthetic groundwater was prepared with an elemental concentration based on the analysis of the groundwater sampled 1999-04-08 in the TRUE Block Scale borehole section KI0025F02, 73.3–77.25 m (Structure #20, Andersson et al. 2002a). The groundwater composition is given in Table 2-4.

Table 2-4. Composition of the synthetic groundwater used in the sorption experiment.

	(mg/kg)		(mg/kg)
Li^+	0.89	F^-	1.2
Na^+	2,070	Cl^-	5,540
K^+	8	Br^-	32.9
Rb^+	0.029	SO_4^{2-}	323
Cs^+	0.002	Si	4.8
Mg^{2+}	43.1	HCO_3	22
Ca^{2+}	1,430	S^{2-}	0.03
Sr^{2+}	19.6		
Ba^{2+}	0.059	pH	7.6[B]
NH_4^+	0.046		
Fe^{2+}	0.1		
Mn^{2+}	0.29		
Ra^{2+}	5E–5[A]		

[A] Only in the samples where Ra tracer was added, otherwise zero.

[B] pH set in the prepared synthetic groundwater, no measurements were performed during or after the rock contact.

The water was prepared by dissolving all major component salts in distilled water (>18 MΩm) at ambient laboratory conditions. After transferring the water into the glovebox (followed by a thorough bubbling of the water with nitrogen gas inside the glovebox) the redox-sensitive components Fe^{2+}, Mn^{2+} and S^{2-} were added to the water. Finally, the $NaHCO_3$ salt was added; thereafter no bubbling of the water was done and an air-tight lid was placed on the flask where the water was stored.

The ammonium acetate and EDTA solutions (applied for the different desorption studies) were prepared by dissolving the salts in distilled water, transferring them into the glovebox and bubbling them thoroughly with nitrogen gas before contacting with the geologic material.

2.2.2 Pre-equilibration

One gram of dried fault gouge material was weighed in a 5 ml centrifugation tube. Exceptions were made for some samples (cf. Table 2-5) where very small amounts of material were available and the experiments thus had to be made in a smaller scale. After the material had been weighed up, 1 ml distilled water was added to the samples, after which they were transferred into the nitrogen-fed glovebox where the experimental activities were performed.

After the fault gouge samples had been transferred into the glovebox, 4 ml of synthetic groundwater was added to the samples. Exchange of the water phase (i.e. mechanical shaking, removal of as much water as possible and adding of 4 ml synthetic groundwater, all processes controlled by weighing) was performed three times before the addition of tracers. In the final solutions, <0.1% of the originally added distilled water were left in the samples. A total pre-equilibration time of 48 days was employed for the fault gouge sorption samples.

The rim zone samples (cf. Table 2-6) were instead transferred directly into the glovebox (i.e. without addition of distilled water). Since the crushed and sieved rim zone materials were not available as early as the gouge material, a pre-equilibration time of only 3 days was employed and only one water exchange was allowed for these materials. The aim was to start the batch experiments at the same time (necessary for coordination due to the use short-lived radioisotopes) and therefore one had to compromise with the pre-equilibrium time for the rim zone material.

The desorption samples (ammonium acetate, EDTA and distilled water, cf. Table 2-5) were, in the case of fault gouge samples, transferred into the glovebox in contact with 1 ml distilled groundwater. In the box, 4 ml of the desorption solutions was added directly to the samples. For the rim zone samples, desorption with ammonium acetate was performed by placing the rock samples into the glove box (i.e. without contacting them with distilled water) and directly contacting them with desorption solutions.

2.2.3 Blank samples

For all types of water phases, a parallel blank sample (water phase without any rock material added) was prepared and was treated exactly the same way as all the corresponding samples with rock material. These samples were to be tagged with tracer, in the same way as for the rock-water samples, and to be used as control samples for quantifying potential sorption due to loss on the polypropylene test tube walls.

2.2.4 Addition of tracer

Tracer stock solutions were prepared by adding appropriate amounts of the different radionuclides into a small amount (10–50 ml) of synthetic groundwater. This preparation was performed at ambient laboratory conditions (i.e. not in the glovebox) and no HCO_3^-, Fe^{2+}, Mn^{2+} and S^{2-} were thus present in the water at this stage. The following stock solutions were prepared:

- Sorption and desorption studies of fault gouge material;
  - Cocktail solution containing $^{22}Na^+$, $^{86}Rb^+$, $^{85}Sr^{2+}$, $^{137}Cs^+$, $^{133}Ba^{2+}$ and $^{54}Mn^{2+}$. The sorption of these tracers was measured using γ-spectrometry, i.e. all tracers could be quantified by simultaneous measurement.
  - Solution containing only $^{45}Ca^{2+}$, measured using liquid scintillation.
  - Solution containing only $^{226}Ra^{2+}$, measured using liquid scintillation with Pulse Shape Analysis (PSA, cf. Byegård et al. 2002). Only for the 1–2 mm fraction.

- Sorption and desorption of rim zone material;
  - Cocktail solution containing $^{86}Rb^{+}$, $^{85}Sr^{2+}$, $^{137}Cs^{+}$ and $^{133}Ba^{2+}$. The sorption of these tracers was measured using γ-spectrometry, i.e. all tracers could be quantified by simultaneous measurement.
  - Solution containing only $^{22}Na^{+}$, measured using γ-spectrometry. (Expectations of very low sorption demanded high activities which would cause interferences in a multi-tracer cocktail). Only for the 1–2 mm fraction.
  - Solution containing only $^{45}Ca^{2+}$, measured using liquid scintillation. Only for the 1–2 mm fraction.
  - Solution containing only $^{226}Ra^{2+}$, measured using liquid scintillation with PSA. Only for the 1–2 mm fraction.

After addition of the radioactive tracers to the stock solutions, the solutions were transferred into the glovebox. Additions of NaOH (in order to compensate for the HCl included in the different tracer solutions), HCO_3^{-}, and the redox-sensitive elements (Fe^{2+}, Mn^{2+} and S^{2-}) were all made inside the box.

Injections of the tracers to the rock/water samples were performed by adding only 3 ml of synthetic groundwater to each sample during the last water exchange. This addition was followed by an addition of 1 ml tracer solution.

2.2.5 Sorption experiment samples

The samples were thoroughly shaken after the addition of tracers and were thereafter shaken regularly. The total contact time employed for the sorption experiment was 129 days for the fault gouge material samples and 122 days for the rim zone samples. After this time, the sample was centrifuged and the water phases were sampled.

For the samples containing tracers that were to be measured by γ-spectrometry, as much water phase as possible was removed from the samples. The sample was thereafter weighed and the amount of water phase left in the rock sample was determined. An equal amount of the sampled water phase was thereafter added to a test tube spiked with the same amount of silica as in the rock sample.

From the samples containing tracers that were to be measured with liquid scintillation (i.e. $^{45}Ca^{2+}$ and $^{226}Ra^{2+}$) the sampled aqueous phase was mixed with a scintillation cocktail. The $^{45}Ca^{2+}$ samples were mixed in the proportions 1 ml aqueous phase to 15 ml Emulsifier safe (Perkin Elmer) cocktail in a plastic scintillation vial. The $^{226}Ra^{2+}$ samples were mixed in the proportions 1 ml aqueous phase to ~23 ml Ultima Gold™ (Perkin Elmer), i.e. filling a glass scintillation vial up to the top. For the latter samples, the samples were allowed to stand 1 month before the measurement, this in order to assure a full radioactive equilibrium between $^{226}Ra^{2+}$ and its daughter isotopes, i.e. Rn-222, Po-218 and Po-214. All these four isotopes decay by alfa-emmision, i.e. one thereby registers 4 alfa pulses for each Ra-226 decay.

2.2.6 Samples used for desorption experiment

The desorption samples were treated in the same way as the sorption samples during the sorption phase (cf. Section 2.1.5), except for a slightly longer contact time applied (150 d for the fault gouge samples and 143 d for the rim zone samples). Centrifugation, sampling and removal of water phase were performed as for the samples used for sorption experiment. After removal of as much of the tracer-spiked groundwater phase as possible, an addition of the same volume of distilled water was performed. This rinsing with distilled water was thereafter repeated 3 times, i.e. a total number of 4 rinsing steps with distilled water were performed. The contact time for each distilled water volume was 30 minutes, except for the last volume which was allowed a contact time of 3 hours. Samples were taken from each water volume used in the rinsing procedure.

After the last distilled water phase had been removed from the sample, addition of the same volume of 1 M NH_4Ac (ammonium acetate) was performed. After thorough mixing, the samples were centrifuged and the NH_4Ac phase was sampled after 30 minutes of contact. The samples were thereafter left for 56 d where after which a final sampling according to the procedures described for the sorption samples was performed.

2.2.7 Measurements

All γ-spectrometry measurements were conducted using a HPGe detector with a sample exchanger using the GENIE2000 software (Canberra). Measurements were performed at two different positions:

- At a ~1 dm distance from the detector, applied for the evaluation of the activities of weakly sorbing tracers, i.e. $^{22}Na^{+}$ and $^{85}Sr^{2+}$. Due to the small amount of tracers attached to the solid phase, it was expected to observe only a very low increase in activity in the measurement of the solid phase, compared to the aqueous phase. This relatively long measurement distance was thus applied to minimize any influence of small deviations in geometrical position between the solid and aqueous phase measurements.
- At a ~1 cm distance from the detector, applied for the evaluation of the activities of the more strongly sorbing tracers, i.e. $^{54}Mn^{2+}$, $^{86}Rb^{+}$, $^{137}Cs^{+}$ and $^{133}Ba^{2+}$. Due to relatively strong sorption of these tracers, quite low activities were obtained in the aqueous phase samples and the shorter distance was thus helpful for increasing the measurement efficiency.

The aqueous phase measurements gave, for the most part, so low activities that a considerably higher uncertainty of the sorption coefficient was obtained. For this reason, an enrichment of the aqueous phases was performed according to:

A. For the rim zone samples, enrichment was performed by adding 0.01 g of ammonium molybdenum phosphate (AMP) to all the sampled aqueous phase (~4 ml, exact amount determined by weighing). This gave a >99% isolation of the $^{137}Cs^{+}$ and $^{86}Rb^{+}$ in the samples.

B. For the fault gouge samples, the same AMP isolation was applied as described for the rim zone samples. Furthermore, a co-precipitation separation of $^{133}Ba^{2+}$ and $^{54}Mn^{2+}$ was performed for these samples. This was done by adding dissolved Na_2CO_3 to the samples, precipitating all Ca^{2+} present in the aqueous phase as a $CaCO_3$(s) precipitation (i.e. 0.015 g precipitation for a 4 ml batch).

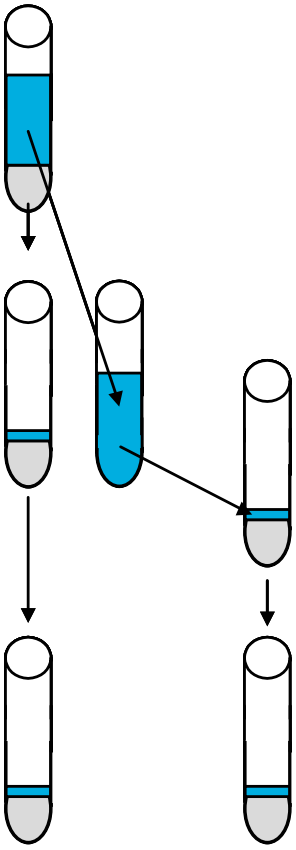

Figure 2-2. *Description of the procedure of solid phase measurements of R_d.*

Table 2-5. Summary of the batch samples included in the investigation of fault gouge materials.

Sample ID and name of associated interpreted structure	Na^+, Rb^+, Sr^{2+}, Cs^+, Ba^{2+} and Mn^{2+}, sorption	Na^+, Sr^{2+}, Cs^+, Ba^{2+} and Mn^{2+}, sorp+desopr	Ca^{2+}, sorption	Ra^{2+}, sorption	1 M NH_4Ac, leaching	0.2 M NH_4Ac, leaching	3E-2 M EDTA, leaching	3E-3 M EDTA, leaching	3E-4 M EDTA, leaching	3E-5 M EDTA, leaching	Distilled water, leaching
1303 (NE-1)	x	–	x	x	–	–	–	–	–	–	–
1596 m (NE-2)	x	x	x	x	x	x	x	x	x	x	x
2169 m	x	–	x	–	–	–	–	–	–	–	–
KAS04 (EW-1)	x	–	x	–	–	–	–	–	–	–	–
KI0025F (Z)	x	x	x	x	x	–	–	–	–	–	–
KI0025F02 (#19)	x	–	–	–	–	–	–	–	–	–	–
KI0023B (#20)	x	–	–	–	–	–	–	–	–	–	–
KI0025F02 (#22)	x	–	–	–	–	–	–	–	–	–	–
KSH02 743 m	x	–	–	–	–	–	–	–	–	–	–

Table 2-6. Summary of the batch samples included in the investigation of rim zone materials (the same amount of samples for all different rock material).

Size fraction (mm)	Rb^+, Sr^{2+}, Cs^+, and Ba^{2+} sorption	Sr^{2+}, Cs^+ and Ba^{2+} sorp+desopr	Na^+, sorption	Ca^{2+}, sorption	Ra^{2+}, sorption	1 M NH_4Ac, leaching
<0.125	x	–	–	–	–	–
0.25–0.5	x	–	–	–	–	–
1–2	x	x	x	x	x	x

3 Evaluation

3.1 Sorption measurements, solid phase measurements

The distribution ratio, R_d (m^3/kg), was determined from the solid phase γ-spectrometry measurements (cf. Figure 2-1), according to:

$$R_d = \frac{1}{\rho_{aq} m_s} \cdot \left(\frac{R_1 \cdot m_{aq(1)}}{R_2} - m_{aq(2)} \right) \quad \text{(Eq 3-1)}$$

where ρ_{aq} is the density (kg/m^3) of the water phase, m_s is the mass (kg) of the geologic material used in the experiment, R_1 is the counting rate (e.g. cpm) obtained for the test tube containing the geologic material, $m_{aq(1)}$ is the mass (kg) of the water phase remaining in the test tube containing the geologic material, R_2 is the counting rate (e.g. cpm) obtained for the test tube containing only water phase together with powdered SiO_2 and $m_{aq(2)}$ is the mass (kg) of the water phase added to the test tube with powdered SiO_2, cf. Figure 2-2.

3.2 Sorption measurements, liquid scintillation measurements

For the liquid scintillation measurements, no direct measurement of the activity of the solid phase was possible. Instead, mass balance was applied, i.e. the sorption coefficient was estimated on basis on the difference of the behavior of the tracers in a sample containing solid phase and a blank sample. The distribution ratio, R_d (m^3/kg), was thus instead calculated according to:

$$R_d = \frac{1}{\rho_{aq} m_s} \cdot \left(\frac{R_0 \cdot m_{aq} \cdot m_{st(aq)} \cdot M_0}{R_{aq} \cdot m_0 \cdot m_{st(0)}} - M_{aq} \right) \quad \text{(Eq 3-2)}$$

where ρ_{aq} is the density (kg/m^3) of the water phase, m_s is the mass (kg) of the geologic material used in the experiment, R_{aq} is the counting rate (e.g. cpm) obtained for the sampled water phase taken from the sample containing the geologic material, m_{aq} is the mass (kg) of this sample, M_{aq} (kg) is the mass of the total amount of water phase in this sample before sampling and $m_{st(aq)}$ (kg) is the mass of the addition of tracer stock solution made to this sample. R_0, m_0, M_0 and $m_{0(aq)}$ are the corresponding parameters for the blank sample, i.e. the sample without any rock material present.

3.3 Definitions of sorption coefficients, R_d and K_d

For the fault gouge material, only the <0.125 mm size fraction were used in the experiments and the sorption distribution coefficient, K_d (m^3/kg), reported is equal to the R_d determined for that size fraction.

For the rim zone material, three different size fractions were used. In the interpretation of the results from these three size fractions, attempts were made to distinguish between the mechanisms of:

- Surface sorption, i.e. sorption interaction between the outer surfaces of the crushed material. Since these outer surfaces are suspected to have been formed during the crushing process, they are often regarded as non-representative for intact rock,
- Sorption caused by diffusion accessing the inner surfaces of the crushed rock particles, i.e. similar to the matrix diffusion process which is considered to be the major retention mechanism in the geosphere for radionuclide transport in the geosphere.

By interpretation of the results according to a model considering the solid phases as consisting of spherical particles of a uniform distribution within the size interval, attempts was made to distinguish between surface distribution coefficients, K_a (m), and mass distribution coefficients, K_d (m^3/kg), according to:

$$R_d = K_d + \frac{6K_a}{\rho_s d_p} \qquad \text{(Eq 3-2)}$$

where ρ_s is the density (kg/m^3) of the solid phase, d_p is the average particle diameter (m). A plot of the three obtained R_d versus 1/ d_p will thus give an intercept equal to the K_d and a slope corresponding to $6K_a/\rho_s$. According to this concept, K_a should account for the crushing induced process of surface sorption while K_a should describe the PA relevant process of sorption interaction with inner surfaces.

3.4 Desorption measurements

3.4.1 Solid phase measurements

An estimation of the percentage of the sorbed tracers that can not be desorbed is made according to:

$$P_{\text{non-des}} = \frac{R_1 - R_2 \cdot \frac{m_1}{m_2}}{R_1 + R_2 \cdot \frac{(m_{\text{tot}} - m_1)}{m_2}} \qquad \text{(Eq 3-5)}$$

4 Results and discussions

The obtained sorption coefficients are given in Table 4-1 for the fault gouge material and Tables 4-2 and 4-3 for the rim zone material and the results are discussed in the following Sections 4.1–4.4. Conclusions drawn from the investigations are presented in Section 4.5

4.1 Fault gouge material

As can be seen in the results, the sorption coefficients are, as can be expected considerably high for the fault gouge material, e.g. due to the small particle size of rock material. The general trend in retention properties between the different tracers observed previously in both laboratory experiments, e.g. Byegård et al. (1998) and *in situ* experiments, e.g. Winberg et al. (2000) and Andersson et al. (2004, 2007), i.e. $Na^+ < Ca^{2+} \approx Sr^{2+} < Ba^{2+} \approx Rb^+ < Cs^+$, seem to be generally confirmed also in this experiment using fault gouge materials. However, there seem to be some more variations in the selectivity for the different tracers than observed in the experiment using crushed major rock types (intact unaltered and altered rock, e.g. Byegård et al. 1998) which indicate that fault gouge material could be a potential source of heterogeneity in retention properties for the various tracers. This heterogeneity could be of importance for the interpretation of the retention observed in *in situ* tracer experiments. Due to the relatively short contact times employed, contact with materials in the closest vicinity of the flowing water in the fracture is expected to determine the retention observed in the breakthrough characteristics.

An interesting observation is that the majority of the fault gouge materials show higher sorption coefficient for Ba^{2+} compared to Rb^+. This is in contradiction with the results of *in situ* tracer experiments at the ÄHRL where simultaneous use of these two tracers, e.g. Winberg et al. (2000) and Andersson et al. (2004), have always shown stronger retention of Rb^+ stronger than for Ba^{2+}. This could be indication that the few materials that have stronger sorption for Rb^+ compared to Ba^{2+} (e.g. 1303 (NE-1)) are representative for the rock material in the vicinity of the flow paths activated during a forced flow tracer experiment. However, due to the low number of referred tracer experiment results, it should be acknowledged that the basis for this indication is very weak.

Comparison of the results for the different tracers shows that especially Cs^+ has a considerable variation in its K_d between the different materials used; the range 0.012–0.37 m^3/kg gives an observed variation of a factor 30. From the mineralogical composition, it is indicated that the presence of mixed layer clay in the samples favors the sorption of Cs^+. The somewhat analogous tracer Rb^+ seems to vary in the same way as Cs^+. However, the large uncertainty associated with this tracer makes it difficult to state any clear conclusions. The reason for the high uncertainty is that the short half-life (18.6 d) caused a considerable decrease in activity during the contact time of the experiment.

For the other commonly used sorbing tracers, the variation between the different geologic materials is not as pronounced as for Cs^+. The Ba^{2+} tracer shows K_d-values in the range of 0.013–0.027 m^3/kg, i.e. a variation only in the order of a factor 2. This can be compared to the results of the other alkaline earth metals, i.e. Sr^{2+} (0.00061–0.0020 m^3/kg) and Ca^{2+} (0.00021–0.0019 m^3/kg) for which the corresponding variations are observed to be in the order of 3 and 10, respectively. The Na^+ shows a corresponding variations in the interval of 0.000056–0.00019 m^3/kg, i.e. in the order of a factor 3.

The Mn^{2+} tracer has so far not been used in the supporting laboratory experiment for the TRUE field experiments. However, it was used in the *in situ* TRUE Block Scale in Experiment, injection C4 (Andersson et al. 2002b, 2004), in which Mn^{2+} showed a behavior indicating sorption strength in between Rb^+ and Cs^+. It was also used as a strongly sorbing tracer in the TRUE Block Scale Continuation 2B experiment (Andersson et al. 2007) where the recovery at the end of the experiment was only 1% (compared to the 92% recovery observed for the non-sorbing tracer of Eu-DTPA).

Somewhat contrary to the *in situ* observations, Mn^{2+} shows the strongest sorption of these tracers for the majority of the fault gouge materials. There is an indication that materials which due to the color indicate a presence of oxidized iron on the surfaces (e.g. the 1596 m (NE-2) material and the KSH02 743 m) favor the selectivity for Mn^{2+} in the sorption. For the two mentioned materials, the K_d for Mn^{2+} is in the order of 3–10 times higher than the corresponding value for Cs^+. Since Mn^{2+} is the tracer in the cocktail that is by far most influenced by hydrolysis, cf. Andersson et al. (2004), it is likely that the strong sorption of Mn^{2+}, correlated to presence of oxidized iron surfaces, can be explained by surface complexation

characteristics. The interaction of divalent metals with different iron oxides has been studied by e.g. Gunnarsson et al. (2000), Marmier et al. (1999) and Rose and Bianchi-Mosquera (1993).

Only for two materials (i.e. the 2169 m material and the KI0025F (Z) material) the same laboratory sorption characteristics are observed as for the *in situ* experiment. For the two materials with the highest K_d for Cs^+ (i.e. 1303 (NE-1) and KAS04 (EW-1)), it is also observed that the K_d for Mn^{2+} is lower than the corresponding value for Rb^+. This observation is in line with the mineralogy; the materials mentioned are the ones with the most pronounced content of mixed layer clay. This mineral group has been considered as being very selective for sorption of K^+, Rb^+ and Cs^+ (e.g. Comans and Hockley 1992) and obviously the strong sorption of these alkali metals can not be correlated to the sorption strength of the other tracers used.

The sorption of Ra^{2+} indicates that this is the strongest sorbing tracer of all tracers included in this work. Only three measurements were available which nevertheless indicates K_d higher than 0.3 m^3/kg for all samples. Carbol and Engkvist (1997) recommend slightly lower K_d for Ra^{2+} than for Cs^+ (0.02 m^3/kg and 0.05 m^3/kg, respectively, for saline groundwater). However, the range is similar and therefore the results must be regarded as being as expected. It is obvious that the experimental technique using very low concentrations of Ra^{2+}, a total concentration 0.05 ppb (~ 8 Bq/ml) and measurements using the strongly selective PSA technique for α–β discrimination, worked out very well. This finding indicates that possible radiation problems using the Ra-226 tracer (degassing of the daughter isotope Rn-222 and thereby exposure of α-activity to the surrounding of the laboratory used) can be handled with the present technique. The selective measurement technique allows use of very low amounts of tracer, still offering possibilities of measurements far above the background level.

An attempt has been made to study the general statistical correlation (R^2) in sorption between the different tracers (Table 4-2). As can be seen, the correlations are in the most cases rather poor. Exceptions are e.g. the correlation between Sr^{2+} and Ca^{2+} ($R^2 = 0.92$) which is expected due to the chemical similarity between Sr^{2+} and Ca^{2+}. The generally low correlations are therefore somewhat contradictory to the hypothesis that the sorption of these presumed cation exchange sorbing tracers should be possible to describe by a simple cation exchange model where the adsorption strength should be solely dependent on the cation exchange capacity of the rock material. It is obvious that a pronounced heterogeneity exists in the selectivity for the different cations, probably caused by the variation in the mineralogy of the different fault gouge materials.

It can therefore be concluded that the composition of the fault gouge material could be a potential source for heterogeneity in the retention; a topic to be addressed in future work, e.g. within the scope of the SKB site investigations at Forsmark and Laxemar-Simpevarp.

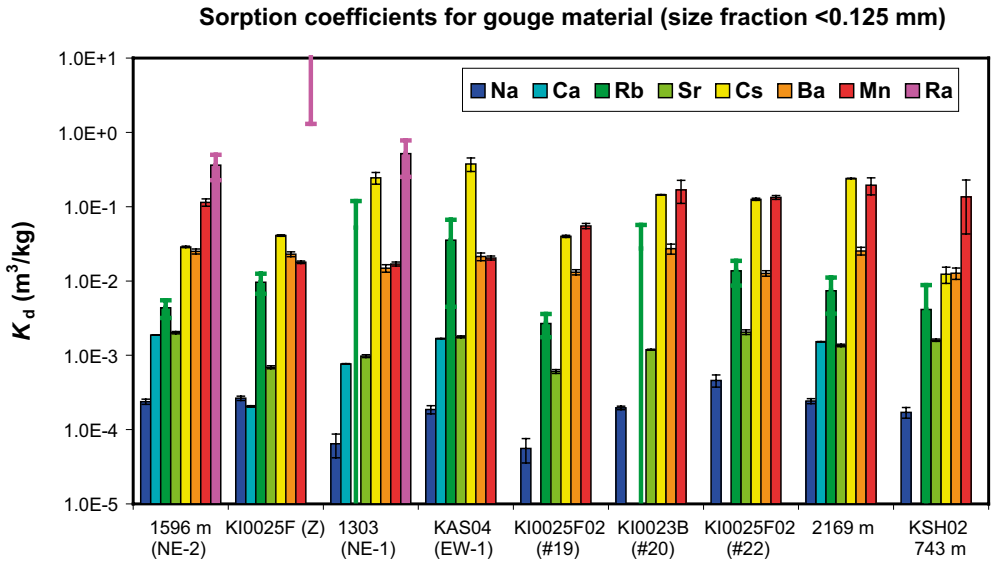

Figure 4-1. *Sorption coefficients for the different fault gouge materials for the different tracers employed in the experiment. For the cases where no activity could be measured in the solid phase (Rb^+ in 1303 NE-1 and KI0023B (#20), mainly due to prolonged radioactive decay) detection limit representing the highest possible K_d is presented in the figure. For the case of Ra^{2+} sorption in the KI0025 (Z) sample, no remaining activity could be found in the water phase and the lowest possible K_d is thus presented in the figure.*

Table 4-1. Sorption coefficient determined for fault gouge material (size fraction <0.125 mm). Contact time was 129 days, except for Ra^{2+} where a contact time of 5 years was applied.

Sample ID and name of associated interpreted geological structure	Na^+		Rb^+		Cs^+		Ca^{2+}		Sr^{2+}		Ba^{2+}		Ra^{2+}		Mn^{2+}	
Material	**K_d (m^3/kg)**	**±**	**K_d (m^3/kg)**	**±**	**K_d (m^3/kg)**	**±**	**K_d (m^3/kg)**	**±**	**K_d (m^3/kg)**	**±**	**K_d (m^3/kg)**	**±**	**K_d (m^3/kg)**	**±**	**K_d (m^3/kg)**	**±**
1303 (NE-1)	6.4E–5	2.3E–5	5.2E–2	6.7E–2	2.4E–1	4.3E–2	7.7E–4	5.4E–6	9.8E–4	4.3E–5	1.5E–2	1.7E–3	5.1E–1	2.6E–1	1.7E–2	1.0E–3
1596 m (NE-2)	2.4E–4	1.9E–5	4.3E–3	1.2E–3	2.9E–2	6.8E–4	1.9E–3	6.4E–6	2.0E–3	7.1E–5	2.5E–2	1.9E–3	3.6E–1	1.4E–1	1.1E–1	1.3E–2
2169 m	2.4E–4	1.9E–5	7.4E–3	3.7E–3	2.4E–1	1.1E–3	1.5E–3	5.9E–6	1.4E–3	5.2E–5	2.5E–2	3.0E–3			1.9E–1	5.0E–2
KAS04 (EW-1)	1.9E–4	2.3E–5	3.6E–2	3.1E–2	3.7E–1	7.7E–2	1.7E–3	6.3E–6	1.8E–3	5.4E–5	2.1E–2	2.5E–3			2.0E–2	1.2E–3
KI0025F (Z)	2.6E–4	1.8E–5	9.6E–3	2.9E–3	4.1E–2	1.0E–3	2.1E–4	4.7E–6	6.9E–4	3.3E–5	2.3E–2	1.7E–3	>1.3E+0		1.8E–2	6.7E–4
KI0025F02 (#19)	5.6E–5	2.0E–5	2.7E–3	9.3E–4	4.0E–2	1.4E–3	–	–	6.1E–4	3.6E–5	1.3E–2	1.1E–3			5.5E–2	4.5E–3
KI0023B (#20)	2.0E–4	1.1E–5	2.7E–2	3.0E–2	1.4E–1	1.1E–3	–	–	1.2E–3	1.7E–5	2.7E–2	4.2E–3			1.7E–1	5.8E–2
KI0025F02 (#22)	4.6E–4	8.5E–5	1.4E–2	5.0E–3	1.3E–1	4.2E–3	–	–	2.0E–3	1.5E–4	1.3E–2	1.1E–3			1.3E–1	8.0E–3
KSH02 743 m	1.7E–4	2.8E–5	4.1E–3	4.7E–3	1.2E–2	3.0E–3	–	–	1.6E–3	5.9E–5	1.3E–2	2.2E–3			1.4E–1	9.3E–2

Table 4-2. Matrix describing the correlation coefficient (R^2) of the sorption of the different tracers on fault gouge material. The correlation coefficients are based on the 5 materials where sorption coefficients were available for all 7 tracers included in the investigation. Ra^{2+} was excluded since only two measured values were obtained in the investigation.

	Na^+	Rb^+	Cs^+	Ca^{2+}	Sr^{2+}	Ba^{2+}	Mn^{2+}
Na^+	–	0.88	0.24	0.01	0.03	0.89	0.20
Rb^+	–	–	0.42	0.03	0.04	0.89	0.40
Cs^+	–	–	–	0.09	0.02	0.15	0.01
Ca^{2+}	–	–	–	–	0.92	0.17	0.29
Sr^{2+}	–	–	–	–	–	0.16	0.13
Ba^{2+}	–	–	–	–	–	–	0.45
Mn^{2+}	–	–	–	–	–	–	–

In the TRUE Block Scale studies (Andersson et al. 2002a) the lack of site-specific sorption data at the time called for predictions of sorption coefficients for the fault gouge materials. In the predictions, a cation exchange model was applied in which the estimated mineralogy and the literature data for cation exchange capacity (CEC) for the minerals were used as data. Besides that, a significant simplification of the concept was introduced by a straight-forward import of selectivity coefficients obtained from evaluation of the sorption on rim zone material from the TRUE-1 site (Byegård et al. 1998). With the application of this concept, no address is made of the heterogeneity in the selectivity caused by variation in the mineralogy. This results in, for a given water composition, that the sorption coefficients will be directly proportional to the CEC and that there will always be a constant ratio between the sorption coefficients for any two given tracers, independent of the mineralogy.

As commented earlier, already the lack of correlation between the sorption coefficients for the different tracers can be considered as an indication of limited validity of the simple cation exchange sorption model as described above. The comparison between predicted and measured K_d -values presented in Figure 4-2 shows that values "correct", at least within one order of magnitude, can be obtained. Generally, an overestimation is obtained for the sorption coefficients of the KI0025F02 (Structure #19) material while the sorption coefficients of the KI0023B (Structure #20) and KI0025F02 (Structure #22) materials are somewhat underestimated. However, considering the uncertainty associated with the data used in the predictions, the results of the predictions should be considered as satisfying given all limitations.

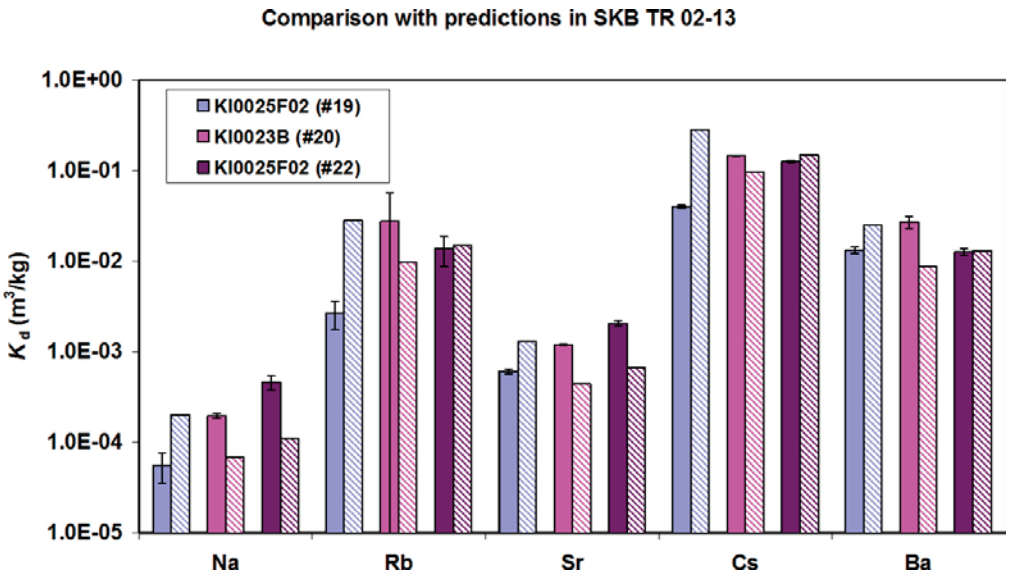

Figure 4-2. *Comparison of the measured sorption coefficients (K_d) and the corresponding predictions made by Anderson et al. (2002b). The solid line bars are the measured values (error bars representing the uncertainty based on counting statistics uncertainty) and the corresponding striped bars correspond to the predicted values.*

Table 4-3. Measured tracer distribution ratios (R_d) for the sorption experiments using fault gouge material (<0.125 mm size fraction), presented in comparison with other Äspö Hard Rock Laboratory investigations using size fraction in the same order.

Experimental campaign		Na^+ R_d (m^3/kg)	Ca^{2+} R_d (m^3/kg)	Rb^+ R_d (m^3/kg)	Sr^{2+} R_d (m^3/kg)	Cs^+ R_d (m^3/kg)	Ba^{2+} R_d (m^3/kg)
Äspö diorite, (Byegård et al. 1998)[A]		1.0E–5[C]	6.3E–5[D]	8.8E–3	1.0E–4[D]	4.1E–1	5.1E–3
Fine-grained granite, (Byegård et al. 1998)[A]		2.7E–5[C]	3.3E–5[D]	3.0E–3	8.4E–5[D]	5.7E–2	3.0E–3
TRUE Block Scale, Fault gouge material, (this work)[B]	Min	5.6E–5	2.1E–4[E]	2.7E–3	6.1E–4	1.2E–2	1.3E–2
	Max	4.6E–4	1.9E–3[E]	5.2E–2	2.0E–3	2.7E–1	2.7E–2

[A] Contact time 14–36 d, size fraction 0.045–0.090 mm. Sorption measured from the tracer loss in the water phase unless indicated otherwise.

[B] Contact time 129 d. Sorption measured from comparative measurements of both the aqueous and solid phase measurements according to the procedures described in this work, unless indicated otherwise.

[C] Comparative measurements of both the aqueous and solid phase measurements after rinsing of the solid phase with distilled water.

[D] Desorption measurements; desorption performed after adsorption followed by a distilled water rinsing of the solid phase.

[E] Sorption measured from the tracer loss in the water phase.

Comparisons have been made of the measured tracer distributions ratios of the fault gouge material to sorption investigation results using crushed igneous rock material in the <0.125 mm size fraction (i.e. same size fractions as used for the gouge material investigation). Generally, the trend is that the sorption on the fault gouge material is higher than for crushed intact and unaltered igneous rock. Based on presented predictions of the CEC on the mineralogy (e.g. Andersson et al. 2002b, Dershowitz et al. 2003) it is expected that the CEC for the fault gouge material should be higher than for intact unaltered wall rock, therefore this finding is not unexpected. The only exception to this trend is for Cs^+ where the high sorption coefficient found for Äspö diorite can not be found in any of the fault gouge materials.

The most pronounced increase of the sorption coefficients of fault gouge material relative to the intact rock is found for the slightly sorbing tracers, i.e. Na^+, Ca^{2+} and Sr^{2+}. However, one need to emphasize that there are some differences in the experimental procedures between the different investigations. Contrary to Byegård et al. (1998), the present investigation applied the solid phase measurement technique (Figure 2-2) so that no rinsing of the solid phase with distilled water had to be applied, as must be done in the desorption measurements technique applied for the weakly sorbing tracers in Byegård et al. (1998). This rinsing process has been suspected to cause desorption of the slightly sorbing tracers (Byegård et al. 1995) which gives suspicions that latter technique underestimate the sorption coefficients . More discussion on this topic is found in Section 4.2 which discusses the results of the sorption on rim zone material.

4.2 Rim zone material

The results of the sorption experiment using crushed rim zone material are presented in Table 4-4 and Figure 4-3 as measured tracer distribution ratios (R_d-values). Details regarding the evaluation concept will be discussed later (cf. Section 4.2.1) where also the evaluated K_d and K_a will be presented.

The order of sorption strength for the different tracers used, $Na^+ < Ca^{2+} \approx Sr^{2+} < Rb^+ < Ba^{2+} < Cs^+$, is the same as for the majority of the fault gouge materials included in the investigation. The trend of stronger sorption for Ba^{2+} relative to Rb^+ is observed for all materials and size fractions, a trend that is in contradiction to the results obtained from *in situ* tracer experiments (cf. Section 4.1). In accordance with the discussion in the previous section, one could thus speculate whether the crushed rim zone material is less representative for the rock material in the vicinity of the flow paths in the *in situ* experiments. However, once again it has to be acknowledged that the amount of data is rather minute for such a conclusion.

Studying the correlation coefficients for the sorption of the different tracers for the rim zone material (Table 4-5) it can be seen that, except for Na^+, much higher values are obtained compared to the corresponding values for fault gouge (cf. Table 4-5). This could be an indication that the sorption characteristics of the rim zone material is generally associated with less heterogeneity in the selectivity compared to the fault gouge material.

There is a variation of the general sorption capacity of the different rim zone materials included in this investigation, cf. Figure 4-3 for comparison of the results from the 1–2 mm size fraction. One of the materials with highest sorption is from the Structure #19 intercept in KI0025F which according to the mineralogical analyses is identified as a strongly hydrothermally altered rock that might contain small remnants of altered biotite. One can compare this to the material from the Structure #19 intercept in KI0023B (a mylonitic and cataclasitic wall rock in Äspö diorite) which is the lowest sorbing rim zone material. This difference is consistent with the difference observed in the measured BET surface area, 0.86 m^2/g for KI0025F and 0.015 m^2/g for KI0023B. However, such high difference as seen for the BET surface (a factor of 60) can not be observed for any K_d -value; the maximum difference is for Cs^+ which differ a factor of 15.

For the two samples from Structure #20 (intercept in KI0023 and KI0025F02, respectively) one can also indentify one comparatively strongly sorbing material (KI0025F02, an altered granitoid with a very thin mylonite closest to the fracture) and one less sorbing material (KI0023, a strongly altered wall rock representing an intermediate variety between cataclasite and mylonite). No BET surface area measurements are available for these materials; the maximum difference in K_d-values is however for Rb^+ for which a difference of a factor 10 is observed. This is contrary to the two #19 samples, where strong alteration does not seem to promote high sorption capacity.

One can thus observe that both for Structure #19 and Structure #20, one rim zone sample with high sorption capacity and one sample with low sorption capacity are obtained. Given this very low number of observations, one can however regard this as an illustration of the difficulty of assigning retention properties to different fractures based on a few number of drill core samples and the necessity of addressing mineralogical heterogeneity when interpreting e.g. an *in situ* tracer experiment.

Regarding the variations between the different tracers, it is indicated that the largest differences are obtained for the Rb^+ and Cs^+ tracers where a variation of from the lowest to the highest values are within a factor of 12 and 15, respectively. The same type of variation for the weakly sorbing divalent tracers (i.e. Ca^{2+} and Sr^{2+}) are a factor of 8 and 6, respectively. The tracer group that seems to be least influenced by rock type variation is that of the stronger sorbing divalent tracers (i.e. Ba^{2+} and Ra^{2+}) where the K_d variation is within a factor of 3.8 and 2.4, respectively.

The obtained tracer distribution ratios for the 1–2 mm fraction are compared to similar data obtained from investigations of fresh and altered Äspö rock types, cf. Table 4-6. The most significant difference between the results of the present investigation and earlier work is that considerably higher sorption is noted for the slightly sorbing tracers, i.e. Na^+, Ca^{2+} and Sr^{2+}. Tracer distribution ratios >1 order of magnitude can be seen.

The reason for this is probably the different measurement technique that has been applied compared to earlier works, i.e. in this work the sorption has been quantified without prior rinsing of the solid phase with distilled water. The results indicate that the rinsing step is causing a significant desorption of slightly sorbing tracers; giving rise to an underestimation of the “real” sorption coefficients. Desorption modelling was performed and discussed by Byegård et al. (1995) and the present investigation strongly indicates that underestimations of sorption coefficients for particularly Na^+, Ca^{2+} and Sr^{2+} may have been obtained in the some of the earlier works.

Table 4-4. Measured tracer distribution ratios (R_d) for the sorption experiment using rim zone material.

Sample ID and name of associated interpreted geological structure	Size fraction (mm)	Na^+ R_d (m^3/kg)	±	Ca^{2+} R_d (m^3/kg)	±	Rb^+ R_d (m^3/kg)	±	Sr^{2+} R_d (m^3/kg)	±	Cs^+ R_d (m^3/kg)	±	Ba^{2+} R_d (m^3/kg)	±	Ra^{2+} R_d (m^3/kg)	±
KI0023B:86 #13	<0.125					4.6E–3	1.1E–3	7.1E–4	3.9E–5	1.1E–1	1.1E–2	2.8E–2	3.7E–3		
	0.25–0.5					2.1E–3	4.5E–4	2.3E–4	2.5E–5	1.8E–2	4.9E–4	6.6E–3	4.6E–4		
	1–2	1.8E–5	1.0E–5	8.9E–5	4.5E–6	6.6E–4	1.7E–4	1.5E–4	2.1E–5	8.1E–3	3.1E–4	3.8E–3	2.5E–4	3.1E–2	2.3E–3
KI0023B:111 #19	<0.125					2.1E–3	5.2E–4	5.5E–4	3.3E–5	3.7E–2	2.1E–3	2.2E–2	3.0E–3		
	0.25–0.5					6.2E–4	1.9E–4	1.0E–4	2.3E–5	5.1E–3	1.8E–4	4.1E–3	2.5E–4		
	1–2	1.5E–5	1.0E–5	4.2E–5	4.4E–6	1.9E–4	6.2E–5	6.1E–5	1.9E–5	2.2E–3	8.3E–5	1.7E–3	1.1E–4	1.7E–2	2.3E–3
KI0025F:166 #19	<0.125					1.7E–2	7.2E–3	9.3E–4	4.6E–5	3.6E–1	6.9E–2	3.1E–2	5.1E–3		
	0.25–0.5					4.6E–3	1.3E–3	2.7E–4	2.6E–5	6.3E–2	4.2E–3	7.6E–3	5.5E–4		
	1–2	3.6E–5	9.8E–6	1.5E–4	4.5E–6	2.3E–3	5.3E–4	1.8E–4	2.1E–5	3.2E–2	1.6E–3	4.3E–3	2.9E–4	2.8E–2	1.9E–3
KI0023B:69 #20	<0.125					2.2E–3	5.4E–4	7.5E–4	4.0E–5	4.2E–2	2.6E–3	2.3E–2	3.1E–3		
	0.25–0.5					5.0E–4	1.4E–4	1.3E–4	2.2E–5	5.8E–3	2.1E–4	3.5E–3	2.0E–4		
	1–2	3.5E–5	9.1E–6	1.9E–5	4.4E–6	2.1E–4	6.6E–5	3.4E–5	2.0E–5	2.1E–3	8.2E–5	1.4E–3	8.8E–5	1.3E–2	7.0E–4
KI0025F02:74 #20	<0.125					4.8E–3	1.4E–3	7.5E–4	4.0E–5	1.8E–1	2.0E–2	2.6E–2	3.3E–3		
	0.25–0.5					2.9E–3	7.6E–4	2.5E–4	2.9E–5	2.6E–2	1.3E–3	8.2E–3	6.5E–4		
	1–2	3.1E–5	9.9E–6	1.2E–4	4.5E–6	2.1E–3	5.4E–4	2.2E–4	2.4E–5	1.5E–2	6.0E–4	5.5E–3	4.3E–4	3.0E–2	2.2E–3
KI0025F02:66 #22	<0.125					4.8E–3	1.2E–3	6.4E–4	3.9E–5	1.0E–1	9.0E–3	2.3E–2	2.2E–3		
	0.25–0.5					2.3E–3	5.7E–4	2.0E–4	2.3E–5	1.8E–2	8.0E–4	5.9E–3	4.3E–4		
	1–2	3.1E–5	1.0E–5	1.2E–4	4.6E–6	9.2E–4	2.5E–4	1.3E–4	2.2E–5	9.1E–3	3.6E–4	3.2E–3	2.1E–4	3.0E–2	2.1E–3

Table 4-5. Matrix describing the correlation coefficient (R^2) of the sorption of the different tracers on rim zone material.

	Na^+	Rb^+	Cs^+	Ca^{2+}	Sr^{2+}	Ba^{2+}	Ra^{2+}
Na^+	–	0.28	0.27	0.01	0.04	0.06	0.00
Rb^+	–	–	0.82	0.78	0.76	0.77	0.42
Cs^+	–	–	–	0.72	0.48	0.46	0.29
Ca^{2+}	–	–	–	–	0.80	0.72	0.74
Sr^{2+}	–	–	–	–	–	0.99	0.82
Ba^{2+}	–	–	–	–	–	–	0.75

Table 4-6. Measured tracer distribution ratios from the sorption experiment using rim zone material (1–2 mm fraction) and comparison to results of other Äspö Hard rock laboratory investigations using batch sorption technique.

Investigation campaign		Na^+ R_d (m^3/kg)	Ca^{2+} R_d (m^3/kg)	Rb^+ R_d (m^3/kg)	Sr^{2+} R_d (m^3/kg)	Cs^+ R_d (m^3/kg)	Ba^{2+} R_d (m^3/kg)
Äspö diorite, (Byegård et al. 1998)[A].		7E–6[D]	4.2E–5[E]	2.8E–3	3.6E–5[D]	5.3E–2	1.1E–3
Fine-grained granite, (Byegård et al. 1998)[A].		5E–6[D]	1.2E–5[E]	8.6E–4	1.8E–5[D]	8.3E–3	7.5E–4
TRUE-1 Feature A Rim zone material, mylonite, (Byegård et al. 1998)[B].	Min	2.6E–6[E]	1.7E–5[E]	2.0E–3	2.6E–5[E]	1.2E–3	0.4E–3
	Max	6.8E–6[E]	2.7E–5[E]	2.0E–3	5.0E–5[E]	8.0E–3	1.3E–3
TRUE-1 Feature A Rim zone material, altered granite/diorite, (Byegård et al. 1998)[B].	Min	1.1E–6[E]	<2E–5[E]	<6E–4	1.0E–5[E]	1.5E–3	4E–4
	Max	4.4E–6[E]	2.7E–5[E]	9E–4	9.0E–5[E]	1.1E–2	1.2E–3
TRUE Block Scale, Rim zone material, (this work)[C].	Min	1.5E–5	1.9E–5[F]	1.9E–4	3.4E–5	2.1E–3	1.4E–3
	Max	3.6E–5	1.5E–4[F]	2.3E–3	2.2E–4	3.2E–2	5.5E–3

[A] Contact time 14–36 d. Sorption measured from the tracer loss in the water phase unless other notification, unaltered rock material.

[B] Contact time 8 d. Sorption measured from the tracer loss in the water phase unless other notification.

[C] Contact time 122 d. Sorption measured from comparative measurements of both the aqueous and solid phase measurements according to the procedures described in this work, unless other notification.

[D] Comparative measurements of both the aqueous and solid phase measurements after rinsing of the solid phase with distilled water.

[E] Desorption measurements; desorption performed after adsorption followed by a distilled water rinsing of the solid phase.

[F] Sorption measured from the tracer loss in the water phase.

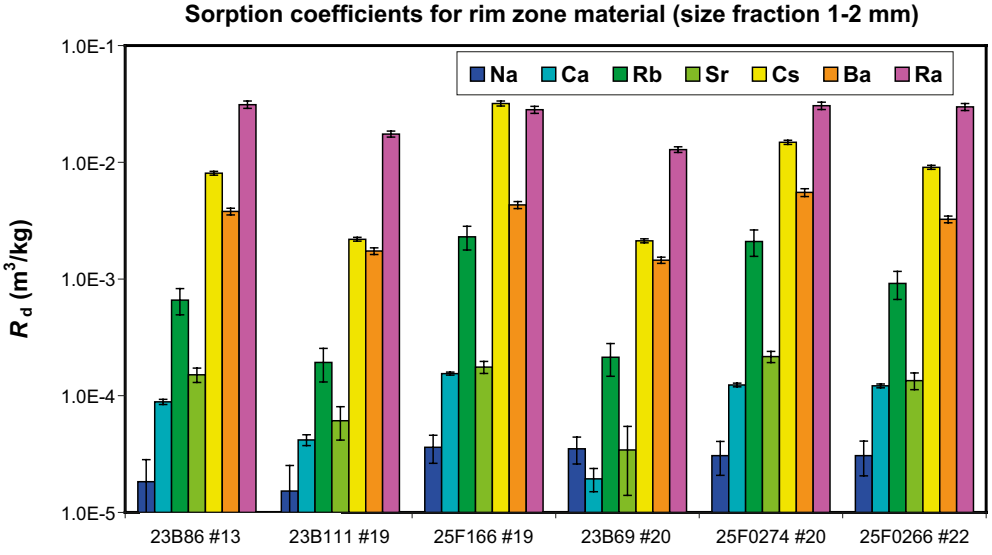

Figure 4-3. *Sorption coefficient (R_d for the 1–2 mm size fraction) for the different tracers rim zone material.*

4.2.1 Evaluation according to the inner/outer surface sorption concept

The results of the evaluation of the different tracer distribution ratios to an inner/outer surface sorption model (cf. Section 3.2) are presented in Table 4-7 (inner surface sorption coefficients, K_d) and Table 4-8 (outer surface sorption coefficients, K_a). A general evaluation of the suitability of the inner/outer surface sorption concept can be obtained by comparing the correlation coefficients (R^2) for the fitting of the proposed model to the experimental data. Although the number of data points used for the estimations is limited, the correlation must be considered as good. For all materials and different tracers used, a pronounced dependence of the inverse of the particle size on the measured tracer distribution ratio (R_d) is observed.

Two examples of fitting the results to an inner/outer surface sorption model are given. The first example (Figure 4-4) is the sorption of Sr^{2+} on the KI0025F02 #22 material for which a linear dependence of the sorption versus the geometrical surface is illustrated very well. The good fit to the linear model yields that an intercept with comparatively low uncertainty can be obtained from the extrapolation.

The second example (Figure 4-5) shows the sorption of Cs^+ on KI0023B #19 material. In this case, the fit is not perfect which causes a significant uncertainty to the results. An interesting observation is that a strict extrapolation yields a negative K_d which of course is physically impossible. However, considering the uncertainties, it is shown that the K_d obtained will be $<8 \cdot 10^{-4}$ m^3/kg. Nevertheless, it is an interesting observation that a strict application of the evaluation concepts will result in a conclusion that no inner surfaces sorption interaction can be verified, i.e. that all sorption interaction observed is on outer surfaces caused by the crushing process.

Comparison of the R_d for the <0.125 mm fraction with the extrapolated K_d can be considered as a measure of the amount of outer surface sorption interaction in relation to the inner surface interaction. The results, cf. Table 4-9, indicate that the major part of the interaction takes place on outer surfaces, i.e. to surfaces that according to this concept are created during the crushing process. The estimation indicates that the stronger sorbing tracers (e.g. Cs^+) are more associated with outer surfaces while the weakly sorbing tracers (e.g. Sr^{2+}) shows a larger amount of sorption on inner surfaces. This observation is consistent with a model where the inner surfaces can only be reached by diffusion. Strongly sorbing tracers are thus suspected to have short penetration depth and are thus expected to have a sorption mostly associated with outer surfaces. The lower sorption, the larger penetration depth and the more emphasized association with inner surfaces is to be expected. However, this could be an indication that sorption equilibrium has not been reached for the strongest sorbing tracers. Therefore, the comparisons of the sorption results to alternative conceptual models are done in the following sections.

An interesting observation is that there is a rather consistent order of the proportion of outer surface sorption between the different rock materials. For example, the material from Structure #20 in KI0023B has the highest amount of outer surfaces among all tracers while the sample from Structure #20 in KI0025F02 seems to be the material that has the largest part of inner surface interactions of all materials.

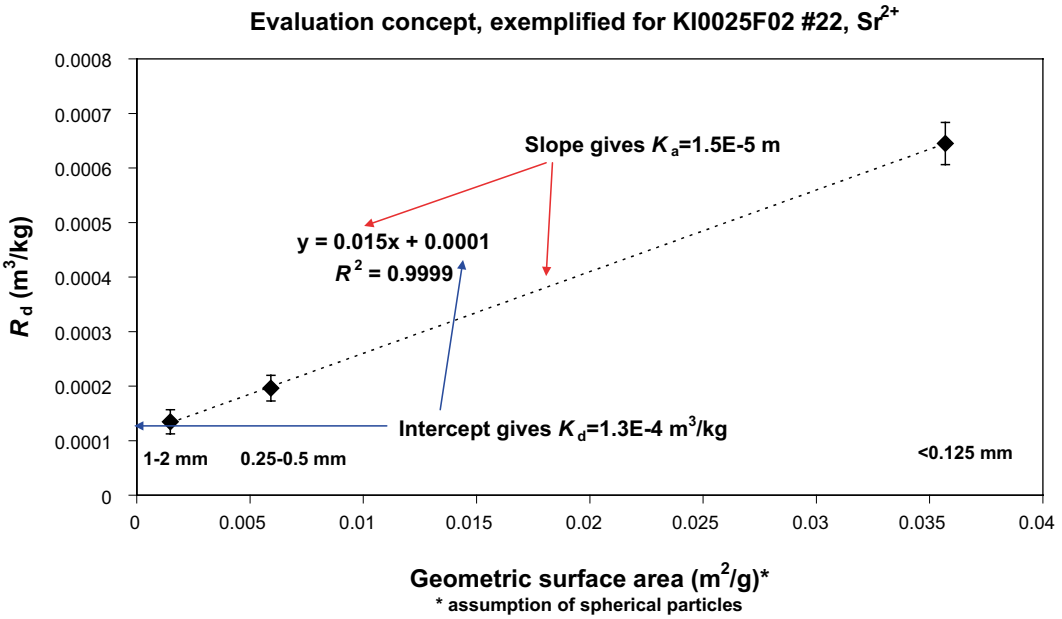

Figure 4-4. Illustration of the evaluation concept according to the outer/inner surface sorption model (cf. Section 3.3), applied for sorption of Sr^{2+} on the KI0025F02 #22 rim zone material.

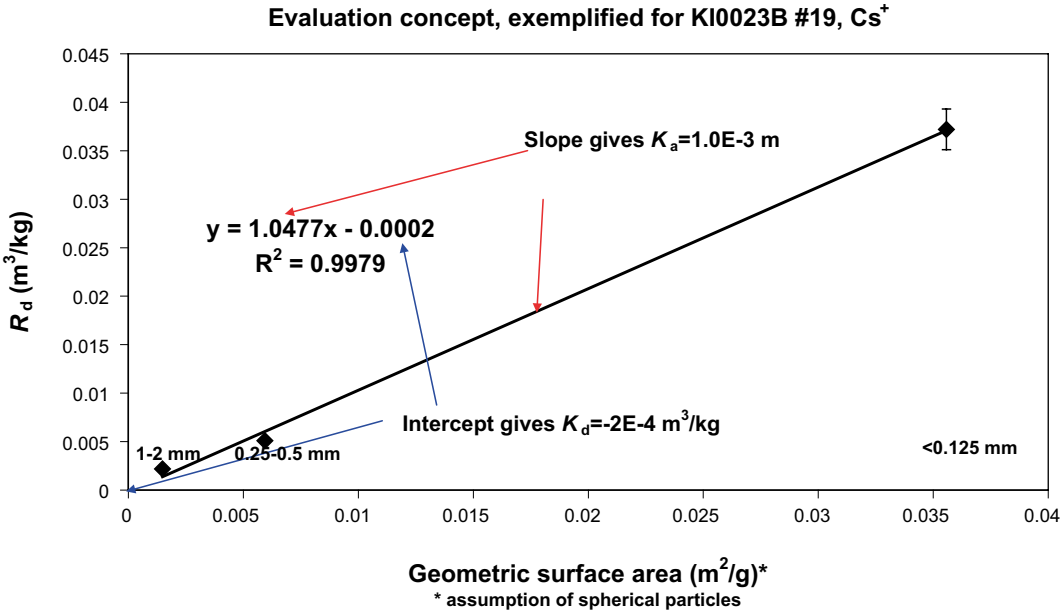

Figure 4-5. Illustration of the evaluation concept according to the outer/inner surface sorption model (cf. Section 3.3), applied for sorption of Cs^{+} on the KI0023B #19 rim zone material.

Table 4-7. Sorption coefficient (K_d) determined for rim zone material. Contact time was 122 days. The values were obtained from an application of the inner/outer-surface extrapolation of 3 size fractions. An exception has been made for Na^+, Ca^{2+} and Ra^{2+} (only 1–2 mm fraction available) where the tracer distribution ratio for 1–2 mm faction has been directly assigned as the K_d.

Sample ID and name of associated interpreted geological structure	Na^+ K_d (m^3/kg)	±	Rb^+ K_d (m^3/kg)	±	Cs^+ K_d (m^3/kg)	±	Ca^{2+} K_d (m^3/kg)	±	Sr^{2+} K_d (m^3/kg)	±	Ba^{2+} K_d (m^3/kg)	±	Ra^{2+} K_d (m^3/kg)	±
KI0023B #13	1.8E–5	1.0E–5	9.5E–4	5.3E–4	2.6E–3	1.4E–3	8.9E–5	4.5E–6	1.3E–4	5.4E–6	2.5E–3	2.3E–4	3.1E–2	2.3E–3
KI0023B #19	1.5E–5	1.0E–5	2.0E–4	1.1E–4	–1.8E–4	1.0E–3	4.2E–5	4.4E–6	2.7E–5	1.5E–5	6.8E–4	1.9E–4	1.7E–2	2.3E–3
KI0025F #19	3.6E–5	9.8E–6	1.8E–3	2.2E–4	1.2E–2	6.8E–3	1.5E–4	4.5E–6	1.4E–4	1.9E–6	3.0E–3	1.2E–4	2.8E–2	1.9E–3
KI0023B #20	3.5E–5	9.1E–6	1.4E–4	1.5E–5	– 4.0E–4	9.3E–3	1.9E–5	4.4E–6	2.0E–6	1.3E–6	1.5E–4	4.3E–4	1.3E–2	7.0E–4
KI0025F02 #20	3.1E–5	9.9E–6	2.2E–3	2.6E–4	2.2E–3	6.4E–3	1.2E–4	4.5E–6	1.8E–4	1.9E–5	4.7E–3	2.3E–5	3,0E–2	2,2E–3
KI0025F02 #22	3.1E–5	1.0E–5	1.2E–3	5.0E–4	3.6E–3	1.8E–3	1.2E–4	4.6E–6	1.1E–4	2.7E–6	2.5E–3	7.7E–5	3.0E–2	2.1E–3

Table 4-8. Surface sorption coefficient (K_a) determined for rim zone material. Contact time was 122 days. The values were obtained from an application of the inner/outer-surface extrapolation of 3 size fractions, see text for details. R^2 for the correlation of the inner/outer surface model to the data is also given.

Sample ID and name of associated interpreted geological structure	Rb^+ K_a (m)	±	R^2	Cs^+ K_a (m)	±	R^2	Sr^{2+} K_a (m)	±	R^2	Ba^{2+} K_a (m)	±	R^2
KI0023B #13	1.0E–4	2.6E–5	0.94	2.9E–3	6.6E–5	0.9995	1.6E–5	2.6E–7	0.9997	7.2E–4	1.1E–5	0.9998
KI0023B #19	5.3E–5	5.1E–6	0.991	1.0E–3	4.8E–5	0.998	1.5E–5	7.4E–7	0.997	6.1E–4	8.9E–6	0.9998
KI0025F #19	4.3E–4	1.1E–5	0.9994	9.8E–3	3.3E–4	0.998	2.2E–5	9.3E–8	0.99998	8.0E–4	5.7E–6	0.99995
KI0023B #20	5.9E–5	7.2E–7	0.9998	1.2E–3	4.5E–5	0.998	2.1E–5	6.1E–8	0.999992	6.4E–4	2.1E–5	0.998
KI0025F02 #20	7.3E–5	1.2E–5	0.97	5.0E–3	3.1E–4	0.996	1.6E–5	9.2E–7	0.997	5.9E–4	1.1E–6	0.999997
KI0025F02 #22	1.0E–4	2.4E–5	0.95	2.7E–3	8.4E–5	0.9991	1.5E–5	1.3E–7	0.99993	5.7E–4	3.7E–6	0.99996

Table 4-9. Estimation of the amount of sorption in the smallest size fraction (<0.125 mm) that is taking place on the outer surface, according to the outer/inner surface concept.

Sample ID and name of associated interpreted geological structure	Rb^+ % sorp. on outer surface	±	Cs^+ % sorp. on outer surface	±	Sr^{2+} % sorp. on outer surface	±	Ba^{2+} % sorp. on outer surface	±
KI0023B #13	79	13	97	1	81	1	91	1
KI0023B #19	90	6	>97		95	3	97	1
KI0025F #19	89	5	97	2	85	1	90	2
KI0023B #20	94	2	>99		>99		99	2
KI0025F02 #20	54	15	99	4	76	3	82	2
KI0025F02 #22	75	12	96	2	83	1	89	1

4.2.2 Modelling

Under ideal conditions, one should expect that the same ratios of inner and outer surface interactions should exist for the different tracers used for a given rock material. However, as can be seen in the results, there is an indication of increasing inner surface interaction with decreasing sorption strength. This observation is in a way consistent with a diffusive sorption interaction model, implying that strongly sorbing tracers, due to the low apparent diffusivity, can only penetrate a small distance into the rock particles. According to this model, there should be a considerable possibility that, due to the limited experiment time, sorption equilibrium has not been reached for the strongest sorbing tracer and that this effect should be most pronounced for the largest size fractions. This non-equilibrium would thus cause a significant underestimation of the K_d (inner surface interaction) and consequently also result in a slight overestimation of the K_a (outer surface interaction).

A problem is of course that the concept of sorption of spherical particles is rather rough and is only based on an assumption. Since there are no independent results available that can verify the ratio of outer/inner surfaces of the rock material, a not yet addressed uncertainty in the geometric surface area must be acknowledged. Nevertheless, the noted high correlation of the linear dependence of the sorption on the outer surfaces must be considered as an indication of good applicability.

Concept of fully porous particles, no surface effects

The very extreme of the diffusive model is that all surfaces of the crushed rock material are representative for intact rock and that the observation of increased sorption with smaller particle size is an effect of variable availability of these surfaces due to diffusion. An attempt has therefore been made to model the obtained sorption results for the KI0025F02 Structure #22 material according to a homogeneous diffusion sorption model (diffusion according to a spherical model, cf. Byegård et al. 1998, pp 60–61).

In this modelling, the K_d for the Rb^+, Sr^{2+}, Cs^+ and Ba^{2+}, together with the formation factor (F_f) for the diffusion, has been used as the fitting parameters.

The effective diffusivity (D_e) for the different tracers is thus calculated from the tabulated water diffusivities (D_w), according to:

$$D_e = F_f \cdot D_w \qquad \text{(Eq 4-1)}$$

This means that the sorption of the mentioned four tracers is modelled using five fitting parameters.

The result of the model calculation is shown in Figure 4-6. As can be seen, the fit of the model to the experimental data is rather poor and there are considerable systematic deviations of the model compared with the experimental results. The F_f obtained in the calculation ($1.7 \cdot 10^{-6}$) is 1–2 orders of magnitudes lower compared with the results of measurements of the F_m on intact rock (normally performed by through diffusion experiments or by electrical resistivity measurements).

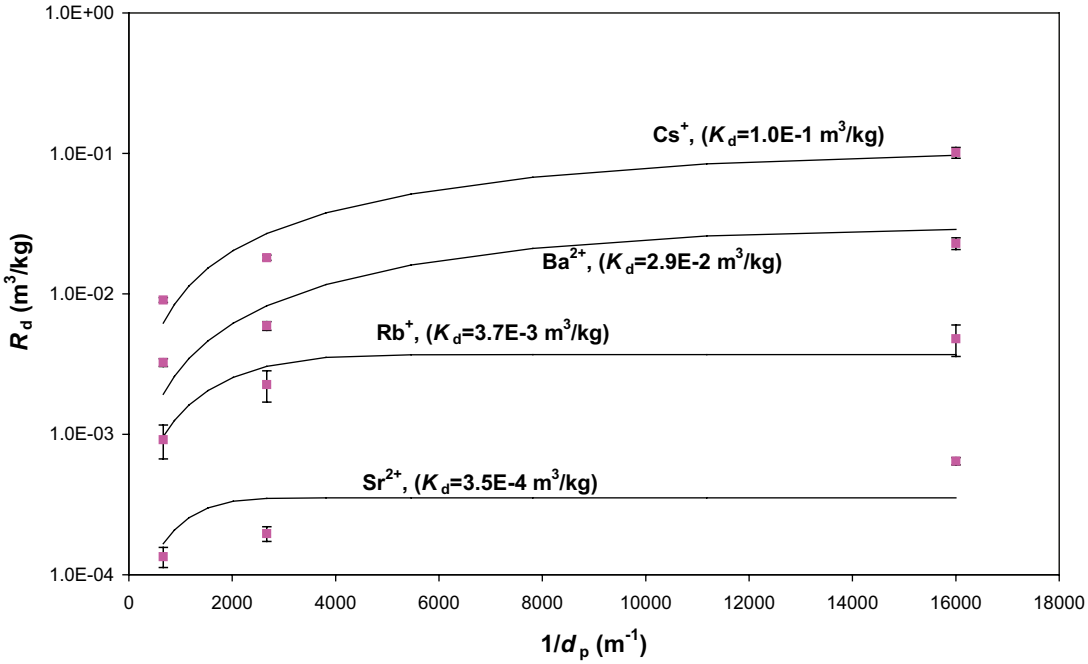

Figure 4-6. *Results of the attempts to simultaneously fit all the sorption results for the KI0025F02 #22 material to a fully diffusive sorption model (see text for details). The obtained K_d-values are presented in the figure and a formation factor (F_f) of $1.7 \cdot 10^{-6}$ was also obtained.*

Nevertheless, the comparatively low D_e obtained for e.g. Sr^{2+} ($1.3 \cdot 10^{-15}$ m^2/s) should according to the model calculation still be enough for obtaining full diffusive penetration of the two smaller size factions within the experimental time applied, i.e. 122 d. This means that two smaller size fractions should show the same tracer distribution ratio (R_d), i.e. a value equal to the K_d. However, there is no such indication in the experimental results for the slightly sorbing tracer Sr^{2+}. On the contrary, a very good correlation of the R_d versus the geometrical surface area is shown for all tracers and there is no indication, whatsoever, of reduced linear dependence with decreasing sorption strength.

The BET surface area measurements of the crushed rock material done within this investigation (cf. Table 2-3) show an significant increase of the BET surface are going from the largest size fraction to the smallest. For the mylonitic and cataclastic rock (KI0023B 111.6 m) an increase from 0.015 to 0.77 m^2/g (i.e. a factor of ~40) is observed while for the strongly hydrothermally altered rock (KI0025 166.65 m) an increase from 0.86 to 2.68 m^2/g (a factor of ~3) is obtained. Furthermore, a large number of the BET surface measurements performed within the SKB site investigation program (e.g. Byegård et al. 2008, Selnert et al. 2009) and BET measurements on major rock types from ÄHRL (Byegård et al. 1998) all indicate that the total surface area is very much dependent on the size fraction of the crushed material. Combining the results from these measurements with the result of the modelling attempt described above, it is obvious that no support of a size fraction independent surface is obtained which therefore contradict the diffusive sorption model.

Time dependence of a combined surface sorption – matrix diffusion model

In this work, it was decided (for reasons of practicality) that only one sampling should be performed during the sorption phase of the experiment, i.e. no information of the variations of sorption with contact time was obtained. However, an attempt has nevertheless made to describe how the sorption should vary with time under applying of the outer/inner surface model.

The calculation is performed according to the diffusive model as referred to above. The only exception is that an instantaneous surface sorption (according to the K_a) has also been incorporated in the calculations. The results for sorption of Ba^{2+} on the KI0025F02 #22 material (i.e. the K_a and K_d values obtained from the inner/outer surface sorption concept, cf. Figure 4-4) were used as input data in the calculation. D_e was selected to obtain the lowest possible value that could fit the obtained experimental data; $D_e=9.2\cdot10^{-14}$ m^2/s was obtained.

The result of the model calculation, cf. Figure 4-7, shows that according to the applied inner/outer surface model the following characteristics should be observed for the experimental results:

- Deviations from the linear dependence should be observed at short contact times and that these deviations should be most pronounced for the larger size fractions.
- Increase of the R_d versus time should be most pronounced for the larger size fractions.
- The smaller size fractions should reach equilibrium within a very short contact time; i.e. no increase in R_d should be observed with increasing contact time.
- Evaluation of the K_a from the slope of the line should yield a slightly decreasing K_a with contact time.

Comparing the model calculation to actual experimental data addressing time dependence in sorption (sorption of Ba^{2+} on Äspö diorite, Byegård et al. 1998), Figure 4-8) shows that there are considerable differences between the model and the experimental results. Actually, the time behavior indicates that the relative increase with contact time is about the same for all size fractions, i.e. a strong contraction to the predicted behavior of the proposed inner/outer surface sorption model. Furthermore, evaluation of the results according to an inner/outer surface concept will yield a rather significant increase in K_a with increasing contact time, which is in contradiction to the conceptual model.

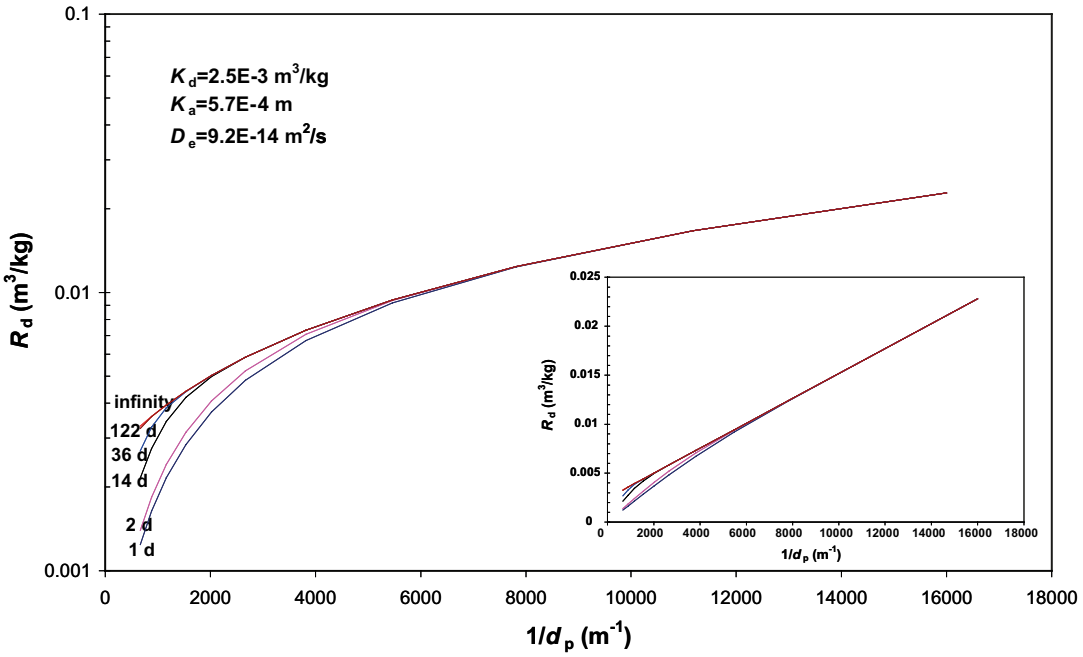

Figure 4-7. *Sorption of Ba^{2+} calculated according to the inner/outer surface model, i.e. instantaneous sorption equilibrium with the outer surfaces and the inner surfaces available by diffusion. The results are presented as R_d given as a function of the inverse particle size for different contact times. Logarithmic and linear presentations are given.*

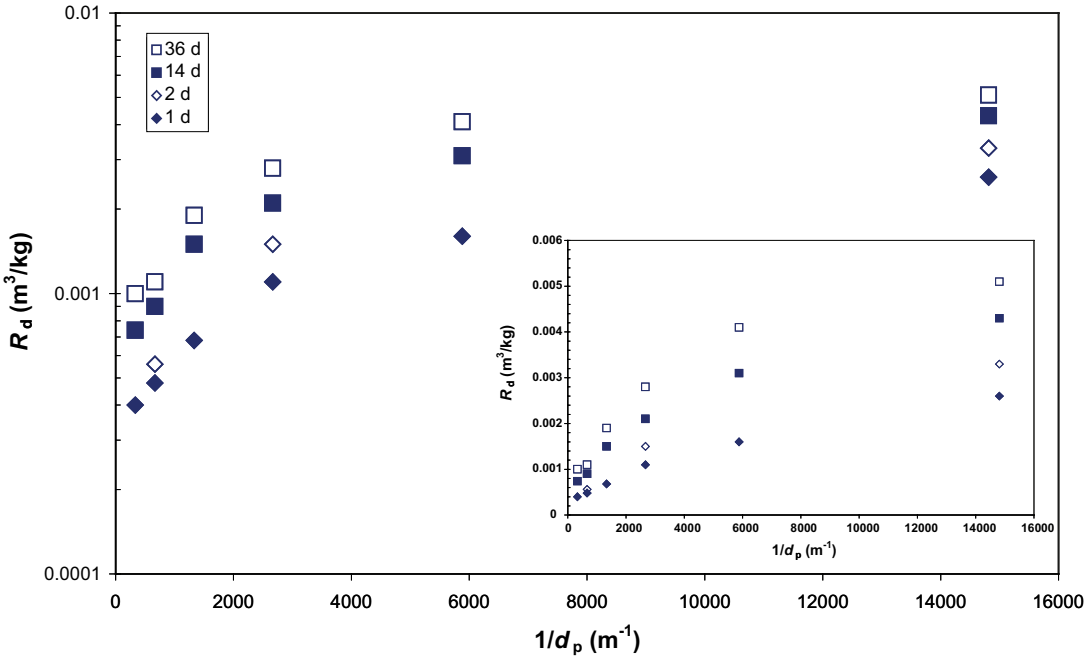

Figure 4-8. *Experimental results of the sorption of Ba^{2+} on Äspö diorite. The results are presented as the R_d given as a function of the inverse particle size for different contact times. Logarithmic and linear presentations are given.*

Concept of fully porous particles (no surface effects) with very low diffusivity

The general mismatch of the experimental results relative to the outer/inner surface model (with respect to the dependence of the sorption on the contact time) makes it necessary to investigate other sorption models. Generally, the increase in R_d for the smallest size fractions even after long contact times could be an indication that a very slow diffusion is taking place in the rock material. The result that even for the relatively moderate sorbing tracer Sr^{2+}, the penetration distance should be extremely low. Consequently, the sorption would, even with very long contact times, be very far from equilibrium.

An attempt to calculate sorption results according to a sorption diffusion model has been performed, i.e. in this case no actual fitting of the model to any experimental results has been performed. In this case, a D_e of $1 \cdot 10^{-17}$ m^2/s has been used. This diffusion rate was selected since this value can still cause linear function of the R_d versus the inverse of the particle with a value of R_d $6.5 \cdot 10^{-4}$ m^3/kg for d_p=16000 m^{-1} at 122 d; i.e. the experimental results for the sorption of Sr^{2+} on the KI0025F02 #22 material.

The results of these calculations are given in Figure 4-9 where presentations of the results for variable K_d) and variable contact time are given. As can be seen, this model consequently produces linear dependence of sorption versus the inverse of the particle size with an intercept zero. Both increasing K_d and increasing contact time give steeper slope of the line, i.e. a very good conceptual agreement with the experimental results.

However, the diffusivity used in these calculations ($1 \cdot 10^{-17}$ m^2/s) is by far much lower than any value determined in any measurement on intact rock, e.g. through diffusion experiments or electrical resistivity measurements. However, one could speculate that the diffusion measured in intact rock, e.g. by through diffusion experiment, to a major extent comprises diffusion taking place in the microfractures and veins between individual mineral grains. This diffusion rate is not unlikely to be significantly higher compared to the diffusion into the mineral grains, which is likely to take place in experiments using crushed rock material.

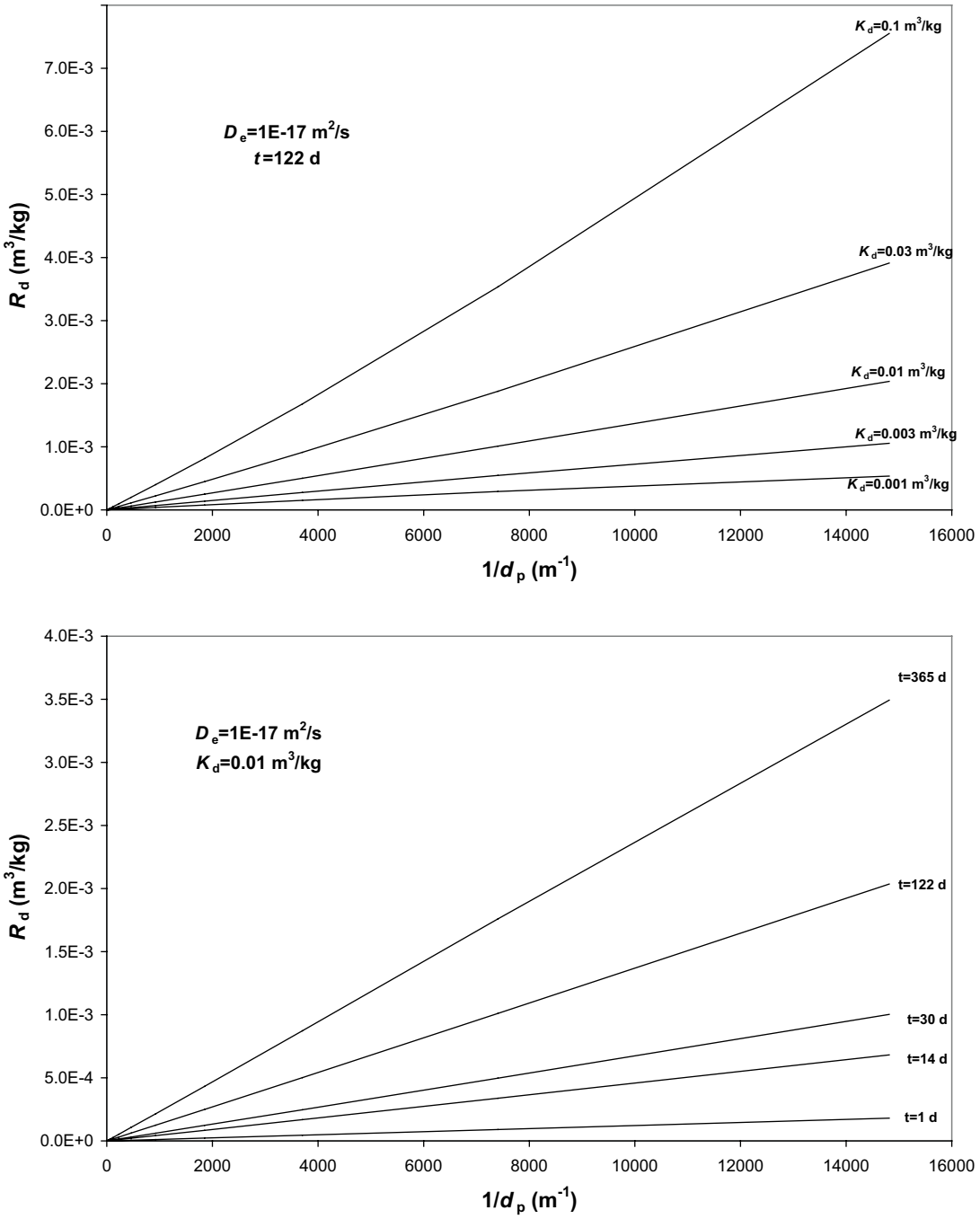

Figure 4-9. *Tracer distribution ratios (R_d) as a function of inverse particle size, obtained from calculations using a spherical diffusion model. Variations of K_d (above) and contact time (below) have been performed.*

As mentioned before, a major disagreement between the diffusion/sorption model and experimental data is that the BET surface measurements show much larger amounts of surfaces for the smaller size fractions than for the larger size fractions (cf. Table 2-3 and e.g. Byegård et al. 2008, 2009). The basic assumption of the diffusion/sorption model is that the total amount of sorption capacity (i.e. the amount of inner surfaces) should be independent of the size fraction measured. However, the extremely low diffusion rate used in these calculations is so low that the possibility of limited penetration of gas diffusion could be anticipated. Theoretically, it is therefore possible that equilibrium is not reached in BET-surface measurements, performed in the time perspective of 1–3 hours. However, no indications of equilibrium problem during these measurements have been observed (Katarina Malaga, SP Technical Research Institute of Sweden, personal communication) and there is also no indication of longer equilibrium times for the larger size fractions compared to the smaller size fractions.

It is obvious that an interpretation of the results calculated with the present model according to an outer/inner surface model (cf. Figure 4-4 and 4-5), yields a significant underestimation of the K_d. Applying the commonly used concept for performance assessment (i.e. neglecting surface sorption, K_a, and only including K_d), this will give a significant underestimation of the retention capacity of the intact rock.

4.3 Desorption experiment

The results obtained from the desorption experiments are presented in Table 4-10 and 4-11. As can be seen, a considerable amount of the sorbed tracers are not desorbed when contacted to a strong electrolyte solution, i.e. 1 M NH_4Ac. Comparing the amount of non-desorbed amounts for the different tracers, there is a rather obvious trend that tracers that are stronger sorbed in the sorption experiments also have a larger part that can not be desorbed with 1 M NH_4Ac. For example, the different rim zone materials show non-desorbed part in the order of; Cs^+ (78–90%) > Ba^{2+} (49–68%) > Sr^{2+} (28–40%). These results are to some extent consistent with the results of Byegård et al. (1995) (sorption studies of Finnsjön granite and chlorite) where the non-desorbed part was found in the order of; Cs^+ (78–92%) > Ba^{2+} (31–36%) > Sr^{2+} (8–10%). In the work of Byegård et al. (1995), a shorter sorption time (7 d) and a shorter desorption time (2 d, 1 M NH_4Ac as desorption medium) were applied. In the investigation of Byegård et al. (1998) (sorption studies on generic Äspö rock material and rim zone material from the TRUE-1 Feature A) desorption was done using non-spiked synthetic groundwater. Also in this work, large portion of non-desorbed tracers were found, especially for Rb^+, Cs^+ and Ba^{2+}. In this current work, other experimental conditions were also employed using a synthetic cation exchanger (Dowex Wx8) as solid phase and the results indicated that all tracer sorption on the cation exchanger was fully reversible.

The only exception to the trend of an increasing portion of desorbed tracer with increasing sorption coefficient is the large portion of Na^+ that can not be desorbed from the KI0025F 194 m (Zone Z) material, an observation that is difficult to explain.

One could speculate that the tracer cations possibly are attached to sorption sites that are extremely selective to the Na^+ cation, i.e. that 1 M NH_4Ac is not sufficient to compete and desorption is therefore not achieved. However, studying the literature review of selectivity coefficients (Bruggenwert and Kamphorst 1982) one can e.g. find that the highest selectivity coefficient for the sorption competition on montmorillonite for Cs^+ versus NH_4^+ is reported at 17.8. With an aqueous concentration of NH_4^+ of 1 M and a sub-ppm concentration of Cs^+ it is obvious that these selectivity data can not explain the non-desorbed portion of the tracers.

Actually, a calculation of the distribution ratios, $R_{d,des}$, obtained for the NH_4Ac desorption step yields significantly higher values than corresponding R_d for the sorption of tracers in a synthetic groundwater environment. This observation of reversed dependence of sorption on ionic strength could at a first glance be interpreted as a sorption process independent of ionic strength. This interpretation would thus contradict cation exchange as the sorption mechanism, i.e. that the sorption would be explained as a phase equilibrium, independent of the water composition. However, comparing the results of the 3 h contact time with distilled water followed by 0.5 hours contact with 1 M NH_4Ac clearly shows the desorption dependence on the electrolyte. It is thus obvious that there is a significant component of cation exchange in the sorption of the tracers used in the current investigation.

A proposed explanation to the non-desorbed portion is that there exists a chemical kinetics effect, i.e. a slow desorption rate. Especially for the Cs^+ interaction with clay minerals, mechanisms have been proposed that involves kinetically hindered desorption. Comans et al. (1991) have proposed that Cs^+ is released from rapidly accessible surface sites and slowly migrates toward a collapsed interlayer site which is more or less resistant to exchange. However, in this work, a general correlation of high initial sorption to a pronounced slow or non-reversible sorption has been established.

In Byegård et al. (1998) attempts were made to explain the sorption and desorption characteristics using a diffusion model including fast and fully reversible cation exchange within the pores of the rock material. The model comprised diffusion into the crushed rock particles during the sorption phase, explaining the time dependence of the R_d observed in the experiments. Furthermore, in order

for desorption to take place, the desorbing agent has to diffuse into the rock particles, exchange with the tracer cations and then diffuse out to the water bulk phase. This double dependence on the diffusion rate would thus make desorption a very slow process and would explain the low portion of the sorbed tracers that could be found in the sampled aqueous phase during the desorption experiments. The results of this modelling indicated that only very low apparent diffusivities (in the order of 10^{-18}–10^{-20} m^2/s) could reproduce the desorption characteristics observed in the experiment. This observation is interesting to compare with the model calculations presented in Section 4.2.2 where it is indicated that the time dependence of the sorption on crushed rock material can also be explained by very low diffusivities into the particles.

Furthermore, in the work of Byegård et al. (1998), attempts were made to model the sorption and desorption according to a first order kinetics model, i.e. explaining the interactions being due to slow chemical reaction rates for sorption and desorption. It was obvious that the desorption characteristics observed in the experimental results could not be explained by this model.

The indication of pronounced limitation of the reversibility in the sorption is actually contradicted by the results of *in situ* experiments. For example, in the TRUE Block Scale experiments (Andersson et al. 2002b), the two most retarded tracers in the C1/C4 injection, $^{54}Mn^{2+}$ and $^{134}Cs^{+}$, have shown recoveries of >85% and >80%, respectively.

This is a very strong indication that the sorption interactions taking place *in situ* are dominated by reversible reactions. It therefore seems difficult to obtain a consistent explanation incorporating both the limitations in reversibility observed in the laboratory studies and the reversible sorption observed in the *in situ* experiments.

An alternative explanation to the limited reversibility could be that a far much more complicated chemical processes than cation exchange are occurring in the rock material during the laboratory experiments, e.g. weathering, oxidation, exposure of water to fresh rock surfaces. If so, this would be a possible indication that the geochemical environment established in the laboratory experiments is not representative of the *in situ* conditions. This of course would raise general doubts of applying data obtained in laboratory batch experiments for performance assessment purposes.

Table 4-10. Percentage of radionuclides that were not desorbed during the different desorption methods applied in this work

Sample ID and name of associated interpreted geological structure	Desorption medium	Desorption time	Na^+ % non-des.	Sr^{2+} % non-des.	Cs^+ % non-des.	Ba^{2+} % non-des.	Mn^{2+} % non-des.
Fault gouge							
1596 m (NE–2)	Distilled water	3 h	31	>99.7	>99.6	>98	>98
1596 m (NE–2)	1 M NH_4Ac	0.5 h	9	8.5	73	46	95
1596 m (NE–2)	1 M NH_4Ac	56 d	6±0.5	7.3±0.1	67±3	40±3	91±8
KI0025F 194 m (Z)	1 M NH_4Ac	56 d	51±2	15±1	38±3	44±4	56±4
Rim zone material							
KI0023B #13	1 M NH_4Ac	56 d	–	27±4	86±2	56±1	–
KI0023B #19	1 M NH_4Ac	56 d	–	37±6	84±2	68±1	–
KI0025F #19	1 M NH_4Ac	56 d	–	34±4	90±1	64±1	–
KI0025F02 #20	Distilled water	3 h	–	>99.4	>99.8	>99.9	–
KI0025F02 #20	1 M NH_4Ac	0.5 h	–	83	95	85	–
KI0025F02 #20	1 M NH_4Ac	56 d	–	29±5	78±1	59±1	–
KI0023B #20	1 M NH_4Ac	56 d	–	40±8	84±2	53±2	–
KI0025F02 #22	1 M NH_4Ac	56 d	–	28±4	81±1	49±1	–

Table 4-11. Sorption coefficients obtained from the desorption experiment ($R_{d,des}$) given in comparison with the corresponding sorption coefficients ($R_{d,sorp}$), the latter corresponding to the values given for the sorption experiment (Tables 4-1 and 4-4)

Sample ID and name of associated interpreted geological structure	Desorption medium	Desorp. time	Na^+ $R_{d,des}$	($R_{d,sorp}$)	Sr^{2+} $R_{d,des}$	($R_{d,sorp}$)	Cs^+ $R_{d,des}$	($R_{d,sorp}$)	Ba^{2+} $R_{d,des}$	($R_{d,sorp}$)	Mn^{2+} $R_{d,des}$	($R_{d,sorp}$)
Fault gouge												
1596 m (NE-2)	Distilled water	3 h	6E–3	2E–4	>3e–1	2E–3	>9E–1	3E–2	>1e–1	2E–2	>3E–1	1E–1
1596 m (NE-2)	1 M NH_4Ac	0.5 h	4E–4	2E–4	4E–4	2E–3	1E–2	3E–2	3E–3	2E–2	8E–2	1E–1
1596 m (NE-2)	1 M NH_4Ac	56 d	3E–4	2E–4	4E–4	2E–3	9E–3	3E–2	3E–3	2E–2	5E–2	1E–1
KI0025F 194 m (Z)	1 M NH_4Ac	56 d	5E–3	3e–4	9E–4	7E–4	3E–3	4E–2	4E–3	1E–2	6E–3	2E–2
Rim zone material												
KI0023B:86 #13	1 M NH_4Ac	56 d	–	–	2E–3	2E–4	3E–2	8E–3	6E–3	4E–3	–	–
KI0023B:111 #19	1 M NH_4Ac	56 d	–	–	3E–3	6E–5	2E–2	2E–3	9E–3	2E–3	–	–
KI0025F:116 #19	1 M NH_4Ac	56 d	–	–	2E–3	2E–4	3E–2	3E–2	7E–3	4E–3	–	–
KI0023B:69 #20	1 M NH_4Ac	56 d	–	–	2E–3	3E–5	2E–2	2E–3	5E–3	1E–3	–	–
KI0025F02:74 #20	Distilled water	3 h	–	–	>2E–1	2E–4	>6E–1	2E–2	>1	6E–3	–	–
KI0025F02:74 #20	1 M NH_4Ac	0.5 h	–	–	2E–2	2E–4	8E–2	2E–2	2E–2	6E–3	–	–
KI0025F02:74 #20	1 M NH_4Ac	56 d	–	–	2E–3	2E–4	2E–2	2E–2	6E–3	6E–3	–	–
KI0025F02:66 #22	1 M NH_4Ac	56 d	–	–	2E–3	1E–4	2E–2	9E–3	4E–3	3E–3	–	–

4.4 Cation exchange, leaching and Cation exchange capacity determinations

4.4.1 Cation exchange capacity

A comparison of the different methods for estimation of the CEC is given in Table 4-12. The methods are:

1. ISO 13536, consisting of:
   a. A saturation step in which the cation exchange sites of the solid material is saturated with Ba^{2+} from a 1 M $BaCl_2$ solution. The amount of leached (desorbed) cations can be measured in this solution and should, assuming an ideal cation exchange behavior, be identical to the cation exchange capacity measured under (b).
   b. An exchange step in which the adsorbed Ba^{2+} is exchanged with Mg^{2+} from a 0.02 M $MgSO_4$ solution according to:

$$Mg^{2+} + Ba\text{-}S_2 + SO_4^{2-} \rightarrow Mg - S_2 + BaSO_4(s) \qquad \text{(Eq 4-2)}$$

where –S refers to a bonding site on the rock material where cation exchange can take place. The amount of Mg^{2+} lost in the aqueous solution is thus a measure of the cation exchange capacity. For a case of an ideal cation exchanger, this amount should balance the amount of desorbed cations under (a).

2. ISO 23470, consisting of a single step in which the solid material is contacted to 0.0166 M $Co(NH_3)_6Cl_3$ (Cobalthexamine trichloride). The trivalent cation $Co(NH_3)_6^{3+}$ is supposed to be strongly adsorbing and thereby in a single step saturating all cation exchange sites and desorbing all formerly attached cations. The cation exchange capacity is thus measured from the aqueous loss of cobalt and the leached cations can be measured in the same solution. Provided a perfect cation exchange behavior, these two numbers should be equal.
3. Provided that the adsorption of cations takes place as a cation exchange mechanism with no net changes in concentration, the results from the batch sorption experiments may be used to estimate the cation exchange capacity. The distribution of a particular added radioactive isotope may thus be regarded as the ratio of that particular element between the solid phase and the aqueous phase. Knowing the total concentration of the element in the aqueous phase and using the assumption that no net change in concentration takes place, the total amount of cations attached to the cation exchange of the solid phase can be estimated. In this particular experiment, no radioisotope tracers were applied for some of the more important cations, e.g. Mg^{2+} and K^+, which means that batch sorption determination of the cation exchange capacity will be an underestimation.
4. In a forth method applied in this work, the solid material is contacted to 1 M NH4Ac (ammonium acetate) in order to extract all cation exchange adsorbed species of the solid material. This resembles the French standard method NFX 31-130 for cation exchange capacity which besides the 1 M NH_4Ac saturation step also includes a ethanol rising step followed by a desorption of the NH_4^+ ions by 1 M NaCl. However, in the present work, only the ammonium acetate extraction step has been employed. The measured extracted amount of cations should, under ideal cation exchange conditions, thus be equal to the cation exchange capacity of the solid material.

All the proposed methods have been applied for the fault gouge material from the NE-2 zone, 1596 m, which enables a comparison of the methods. Given the conditions, a comparatively good agreement is observed between the sorption of Co-hexamine (ISO 23470), desorbed amount of cation (from both ISO 13536 and ISO 23470) and the batch adsorption experiment. These methods yield CEC in the range of 14.8–19.6 cmoles/kg.

A large deviation is observed for the adsorption part of the ISO 13536 which only gives a CEC of 3.7±2.5 cmoles/kg. Considering all the reported values for the different rock material obtained by this method, all values except one are reported below the detection limit. This means that the Mg^{2+} concentration decrease for these samples is below 5% (estimated as the repetitive uncertainty in ICP-AES determination of Mg^{2+}, (ALS Scandinavia, Luleå, personal communication) which produce a detection limit in the range of 2–5 cmoles/kg. However, if the correct CEC would be in the range given by the alternative methods, i.e. in the range of 14.8–19.6 cmoles/kg, a concentration

Table 4-12. Comparison of the different methods used for the estimation of Cation Exchange Capacity (CEC) applied in this work. The numbers are given in the unit cmoles/kg.

Sample ID and name of associated interpreted geological structure	Pre-treatment	ISO 13536, Ba^{2+}/Mg^{2+} sorption		ISO 23470, Co-hexamine sorption		Sorption experiment	Desorbed 1 M NH_4Ac
			Desorbed		Desorbed		
1596 m NE-2	No	3.7±2.5	19.6±1.0	14.8±1.3	16.8±0.8	15.7±0.2[A]	32.4±1.6
	Synt. GW	<4.8	16.6±0.8				
	1 M NH_4Ac	<2.8	(1.2±0.1)[B]				
KI0025F 194 m	No	<3.5	3.8±0.2			3.9±0.2[A]	15.0±0.7
	Synt. GW	<3.1	3.2±0.2				
	1 M NH_4Ac	<5.5	(6.9±0.3)[B]				
1303 NE-1	No					6.1±0.2[A]	
	Synt. GW	<6.2	7.1±0.3				
2169 m	No	<6.6	26.9±1.3			13.3±0.2[A]	
KI0023 111 m #19	No	<2.8	<0.5			0.8±0.4[A]	14.6±0.7
	Synt. GW	<3.9	<0.6				
	1 M NH_4Ac	<2.7	(<0.5)[B]				
KI0025F 166 m #19	No	<4.1	0.6±0.2			0.3±0.1[A]	17.8±0.9
	Synt. GW	<3.2	1.2±0.1				
	1 M NH_4Ac	<3.5	(<0.4)[B]				
KI0023B 69 m #20	No					0.3±0.2[A]	1.4±0.1
KI0025F02 74 m #20	No					0.8±0.4[A]	7.1±0.4
KI0023B 86 m #13	No					0.6±0.3[A]	7.6±0.4
KI0025F02 66 m #22	No					1.0±0.5[A]	

[A] Calculated assuming that the measured adsorption of the radioactive isotopes added ($^{22}Na^{+}$, $^{45}Ca^{2+}$, $^{86}Rb^{+}$, $^{85}Sr^{2+}$, $^{137}Cs^{+}$, $^{133}Ba^{2+}$ and $^{54}Mn^{2+}$) occurs according to a ideal isotope exchange mechanism, i.e. no net changes in the water or the rock phase is occurring. Since no address of e.g. Mg^{2+} and K^{+} is done, the value should be considered as underestimated.

[B] No measurement of desorbed NH_4^{+} was performed and given the pre-saturation with 1 M NH_4Cl a value of zero should be expected.

increase above 5% would have been produced for the 1596 NE-2 zone sample. This indicates that the Mg^{2+} does not fully replace the adsorbed Ba^{2+} from the saturation step and that the ISO 13536 does not seem suitable for determination of CEC for this type of rock material.

The relatively new method ISO 23470 implying studies of the sorption of the Co-hexamine complex looks very promising for this purpose. The result coincides fairly well with both the amount of desorbed cations and also with the results of the batch sorption experiments. Since it only contains one step in which both the losses of Co-hexamine and the amount of desorbed cations are measured, the method is less laborious. With a 5% general uncertainty in the determination of cobalt concentration, one can estimate a general detection limit of this method in the order of 2.5 cmoles/kg. This is not theoretically much more sensitive than the Ba^{2+}/Mg^{2+} method (ISO 13536) and would not be sufficient to measure the CEC of crushed rim zone material (in the range of 0.3–1 cmoles/kg, provided that the estimation using the results of the batch sorption experiment is correct). However, the results from the 1596 m NE-2 zone sample indicates that the selectivity of the Co-hexamine cation is much higher compared to Ba^{2+} replacement of Mg^{2+}.

Furthermore, an additional experiment was performed in which the ISO 23470 prescribed concentration of Co-hexamine of 0.0166 M was decreased by a factor 10. Contacting this solution to the 1596 m NE-2 zone sample gave a >99.99% loss of the Co-hexamine in the aqueous phase; however, this amount was not sufficient for an occupation of more than 2.3 cmoles/kg of the cation exchange sites. This situation corresponds to a sorption distribution coefficient (R_d) for Co-hexamine of >100 m^3/kg which indicate a potential for a revised method in which CEC for low-adsorbing crystalline rock could be determined by adsorption of Co-hexamine used in lower concentration than prescribed by the ISO 23470 method.

The desorption measured after contact to 1 M NH_4Ac show in almost all cases a desorbed amount of cations that does not coincide with any of the alternative estimations of the CEC.

It is indicated that this leaching method gives a desorbed amount of cations that is 2–50 times higher than what is expected from the other methods. Studies the speciation of the adsorbed cation by different methods (Figures 4-10 and 4-11) indicates that high concentration of Ca^{2+} is obtained which could be indicative that not only cation exchange desorption occurs but also a dissolution of calcite, according to:

$$CaCO_3(s) + NH_4^+ \rightarrow Ca^{2+} + HCO_3^- + NH_3 \qquad \text{(Eq 4-3)}$$

The 1 M NH_4Ac thus offers a buffer capacity which can buffer the hydroxide produced in normal conditions of calcite dissolution, which could be a reason for increased dissolution rate.

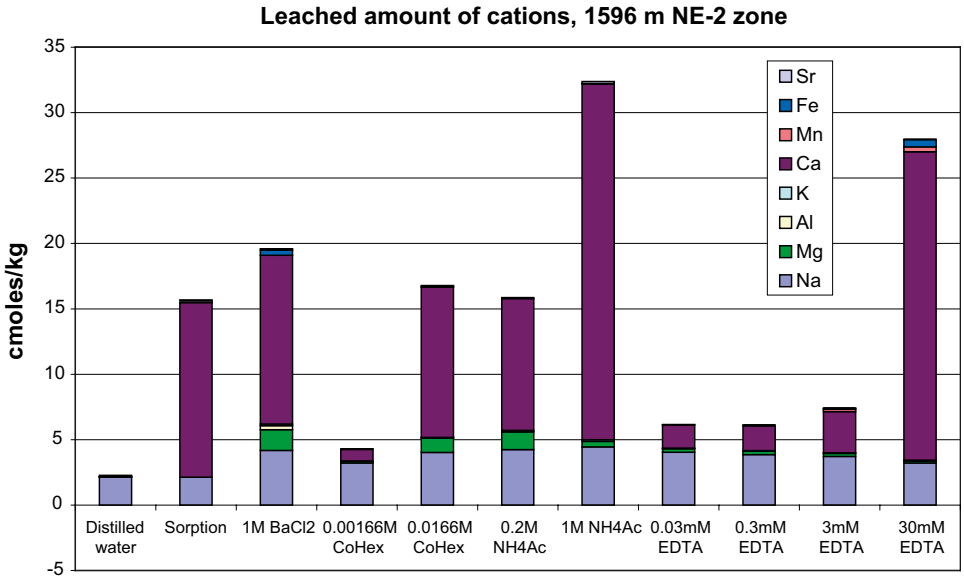

Figure 4-10. *Speciation of the cations desorbed by the different methods used in this work. Results are presented for the experiments using the gouge material from 1596 NE-2 zone.*

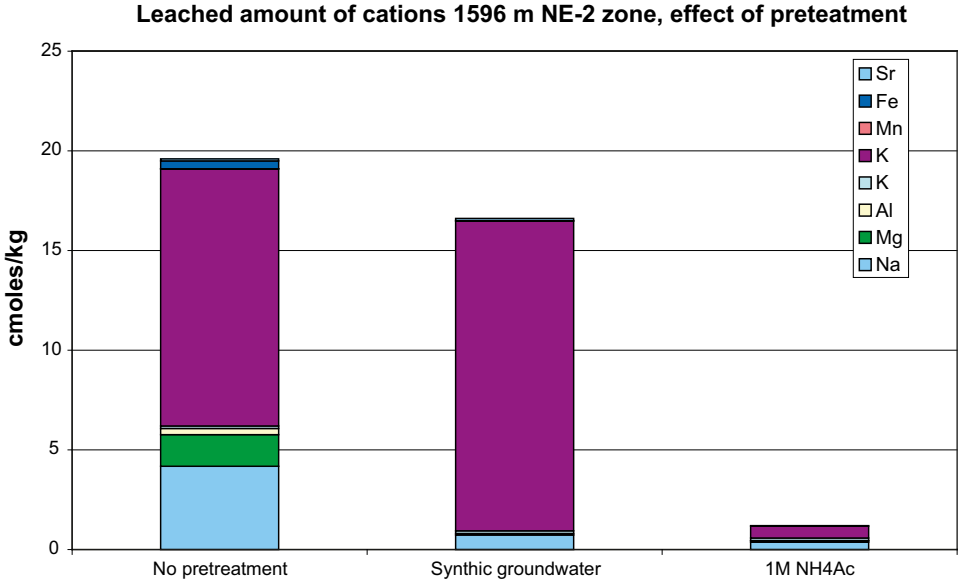

Figure 4-11. *Speciation of the cations desorbed by the 1 M $BaCl_2$ saturation method (ISO 13536). Results are presented for the experiments using the gouge material from 1596 NE-2 zone and illustrate the effect of pretreatment of the gouge material before the leaching, i.e. without pretreatment, 5 years contact with synthetic groundwater and 5 years contact with 1 M NH_4Ac.*

4.4.2 Results of the leaching studies

In Figures 4-10 and 4-11, the speciation of the eluate of the different leaching methods is shown. One can easily realize that Ca^{2+} takes up the absolute major part of the cation leached by the different methods aimed to study the cation exchange mechanism. This is in agreement with similar studies made by Byegård et al. (1995, 1998). One can see that Mg^{2+} as a maximum can occupy 10% of the CEC which indicates that the CEC determined from the results of the batch sorption experiment (where Mg^{2+} sorption is not addressed) is suspected to underestimate the CEC with up to 10%.

The leaching results for Na^+ indicates that this cation occupies 2–4 cmoles/kg of the cation exchange capacity of the 1596 m NE-2 zone material. However, one can observe that comparatively high amounts of Na^+ are desorbed by only contacting the rock material to the distilled water; an observation that somewhat contradict the proposed cation exchange sorption mechanism for this cation. Alternative explanations are that the sodium leached is a result of diffusion from pores in the rock material or that it simply is a result of salt remaining from the groundwater surrounding the rock material that had evaporated. One can see that the results of the batch sorption experiment (which do not address the leaching process) indicates a lower Na^+ occupation in the solid phase compared to the result of the different leaching methods. This supports that at least a half of the Na^+ leached is not a result of cation exchange and that an overestimation of the CEC in the range of 10% is suspected from the results of the leaching methods. Furthermore, in Byegård et al. (1995) a discussion is presented of the possibility of H^+ exchange with Na^+ which also could be an explanation for the Na^+ released from the rock material which is only contacted with distilled water.

Concerning the other cations studied, they are present in very low amounts in the cation exchanged part of the solid phase. This is not unexpected since most of them are present at very low concentrations in the groundwater; even with high sorption distribution coefficient they will not contribute to any significant part to the total amount of cations attached to the CEC.

4.4.3 EDTA leaching

The results of the leaching using the strong complexing agent EDTA (ethylenediamine tetraacetic acid) in combination with 0.07 M LiCl, Figure 4-10, show that large amounts of Ca^{2+} are released from the solid material. Using a EDTA concentration of 30 mM the same amount of Ca^{2+} is released as in the case of 1 M NH_4Ac leaching, i.e. ~20 mM. Based on the discussion above concerning the results of 1 M NH_4Ac leaching, one may conclude that a significant part of this amount of leached Ca^{2+} is not released by cation exchange but is a result of calcite dissolution, according to:

$$CaCO_3(s) + HEDTA^{3-} \rightarrow CaEDTA^{2-} + HCO_3^- \qquad \text{(Eq 4-4)}$$

Actually, the EDTA complexing agent is theoretically strong enough to be suspected to cause dissolution of other rock materials, e.g. aluminum silicates, aluminum oxides and/or iron oxides. However, as can be seen by the results (Figures 4-12 and 4-13), no increase of the silicate concentration can be observed for the EDTA leaching samples. There is, however, an observable increase of the dissolved Al and Fe with increasing EDTA concentration which could be indicative of dissolution of iron and/or aluminum containing solid phases. Since the aim of the EDTA leaching studies was to obtain information whether this technique could be used for surface complexation speciation of the solid phase, the indication of dissolution taking place is somewhat discouraging. The desorption tracer elements (some of them chemical analogues or homologues to element present in spent nuclear fuel) might be argued to have been co-precipitated in e.g. calcite or ferric hydroxides and not (as hypothesized) bound to the solid phase by surface complexation.

Nevertheless, one can not from these results rule out the possibility that the leached Fe and/or Al also is a result of EDTA-induced desorption of surface-complexed Fe and/or Al species; i.e. that desorption of tracer elements is caused by surface decomplexation. In any case, the results indicate a pool of tracer elements that are available for desorption by quite mild desorption methods (i.e. one does not have to dissolve the aluminum silicates by e.g. hydrofluoric acid to transfer them to the aqueous phase). This makes it interesting to address this pool of solid phase-bound tracer elements in K_d estimations, i.e. comparing these solid phase concentrations to the concentration of the tracer elements obtained by only contacting the rock material to synthetic groundwater. Using these tracer distribution ratios as K_d values (cf. Table 4-13) one obtains values that are comparable

to generally accepted values found in the literature. The technique presented and used in this report may be regarded as a "reverse batch adsorption experiment"; as opposed to normal batch sorption technique the tracer is in this case transferred to the system by the solid phase instead of spiking the solid phase. A potential agreement between these two techniques would indicate robustness in the K_d-concept to be applied in performance assessment calculations.

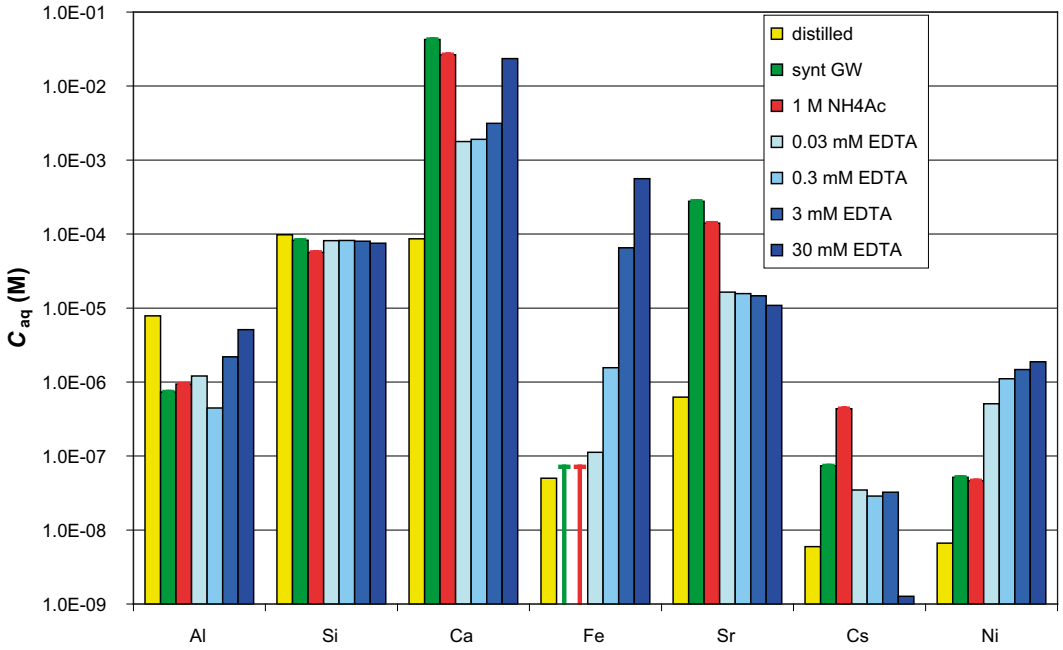

Figure 4-12. *Results of the leaching of the gouge material from the 1596 NE-2 zone, results given for some major components of the rock material (i.e. Al-Fe) and some trace elements (i.e. Sr-Ni). The results are given as the concentration (M) in the water phase of the different elements. In the cases where no concentration of the element could be measured in the aqueous phase, the detection limit is given as an error bar.*

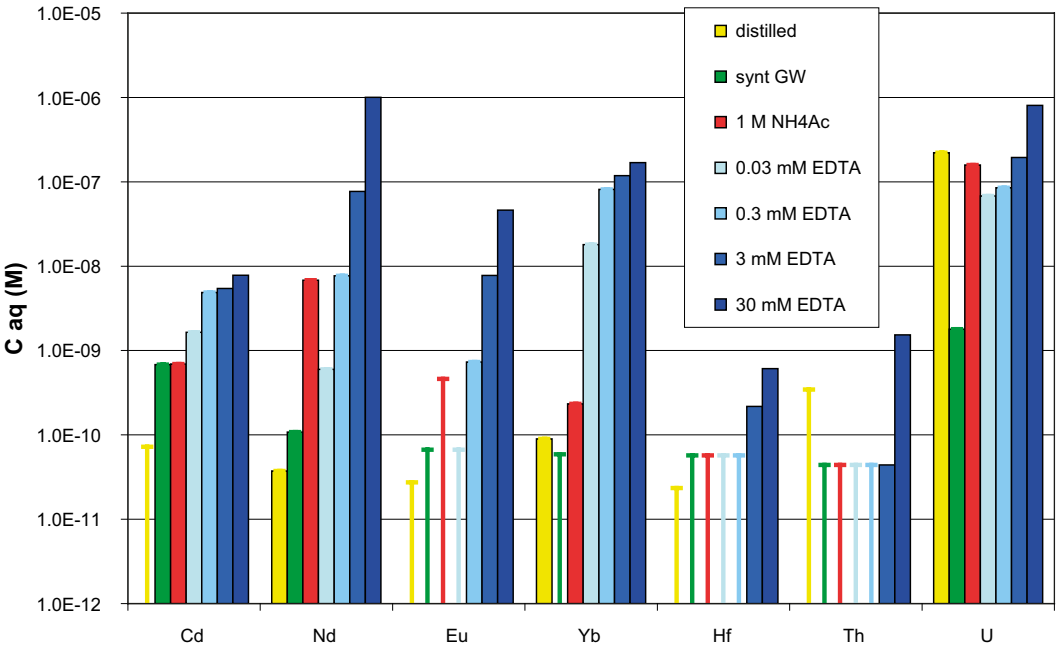

Figure 4-13. *Results of the leaching of the gouge material from the 1596 NE-2 zone, results given for some trace elements. The results are given as the concentration (M) in the water phase of the different elements. In the cases where no concentration of the element could be measured in the aqueous phase, the detection limit is given as an error bar.*

Table 4-13. Maximum leached amount of different element (30 mM EDTA for the presumed surface complexation sorbed tracers, 0.017 M Co-hexamine for the presumed cation exchange sorbing tracers). For comparison, the measured aqueous concentrations of the elements in the batch sorption experiments using synthetic groundwater are presented. The ratio of these two is presented as a K_d (m^3/kg) and these are compared to values determined by the batch sorption experiments in this work and values from a literature review.

	Conc. Batch sorption exp. (M)	Maximum leached[A] (moles/kg)	Corresponding K_d (m^3/kg)[B]	Comparison K_d[C] (m^3/kg)
Al(III)	8E–6	2E–5 (EDTA)	0.03	
Ca^{2+}	4E–2	6E–2 (Co-Hex)	1.3E–3	1.9E–3
Fe(II)	<7E–8	3E–2 (EDTA)	40	
Na^{+}	1E–1	4E–2 (Co-Hex)	0.4E–3	0.2E–3
Rb^{+}	5E–7	4E–6 (Co-Hex)	10E–2	4E–3
Sr^{2+}	3E–4	5E–4 (Co-Hex)	2E–3	2E–3
Cs^{+}	7E–8	4E–7 (Co-Hex)	6E–3	30E–3
Ba^{2+}	1E–6	7E–6 (Co-Hex)	5E–3	30E–3
Mn^{2+}	5E–6	2E–3 (Co-Hex)	0.4	0.1
Ni(II)	5E–8	9E–6 (EDTA)	0.2	0.02
Cd(II)	6E–10	3E–8 (EDTA)	0.04	0.02
Nd(III)	1E–10	5E–6 (EDTA)	50	2
Eu(III)	<7E–11	2E–7 (EDTA)	>4	2
Yb(III)	<6E–11	8E–7 (EDTA)	>10	2
Hf(IV)	<6E–11	3E–9 (EDTA)	>0.05	
Th(IV)	<4E–11	7E–9 (EDTA)	>0.2	5
U(IV)	2E–9	4E–6 (EDTA)	2	5

[A] Results refer to 0.0166 M Co-hexamine for presumed cation exchange sorbing species and to 30 mM EDTA for presumed surface complexation sorbing species.

[B] K_d calculated as the ratio of the leached amount versus the aqueous concentration measured in the water phase in the batch sorption experiment.

[C] Non-italic refers to the batch sorption results in this report, italic refers to the literature study of Carbol and Engkvist (1997).

4.4.4 Changes in groundwater composition due to water-rock phase interaction

A prerequisite for the applicability of the sorption coefficient determined is that the water phase composition is the same in the laboratory experiment as in the *in situ* conditions for which they are to be applied. The tracers used in the batch sorption experiments of this work are presumed to sorb mainly by cation exchange mechanism and the concentration of competitive cations is therefore the most important condition. For this reason, measurement of the aqueous phase after 5 years of contact time has been performed.

Another important condition is the underlying assumption that the rock material is expected to be in a chemical equilibrium with the groundwater, i.e. no extra weathering should occur due to exposure to a water phase composition that is not “natural” for the rock phase. One should consider that the rock material used in this work is from several different locations mainly in the Äspö HRL and that it is possible that the groundwater composition differs somewhat between the different sampling locations. However, the ambition in this work was restricted to mainly address sorbing conditions in the TRUE Block Scale Experiments and hence only one single groundwater composition was used, cf. Chapter 1. One should also have in mind the possibility that sampling from a particular borehole section (e.g. intersecting a particular fracture of interest) may give a water that is a mixture from different part of the fracture (or applicable rock volume, for that matter). Especially the fault gouge material (several of them sampled in other locations than the TRUE Block Scale site) may in their natural location have been in contact with a water with a different composition. Furthermore, the fracture rime zone material is supposed to have mainly been equilibrated with a matrix pore water; a water that do not necessary have to have the same composition as the sampled water.

Especially for the rim zone material, it is also a question if the crushing process opens up new fresh surfaces that have not been equilibrated to groundwater. This is not presumed to be the case for the fault gouge material which has been sampled in a unconsolidated state and has not undergone any additional crushing process after the sampling.

The results of the water phase measurements are given in Table 4-14. A significant difference can be seen when comparing the measured water composition in relation to the recipe, i.e. the ground water composition measured *in situ* relative to the synthetic groundwater composition aimed for. The increase in the measured water versus the recipe of 2–5% observed for the major cationic components (i.e. Na^+ and Ca^{2+}) is an indication of an evaporation. Besides, considering a 5% general repetitive uncertainty in the measurement (ALS Scandinavia, Luleå, personal communication) these values may be within the expected uncertainty. The other increases relative to the recipe should probably be to impurities in the salts used for manufacturing the synthetic groundwater.

When comparing the results of the measurement of the blank sample of synthetic groundwater with the different waters that have been in contact with rock material, a general trend is noticed where the salt content increases as a consequence of the rock contact. For the major salt components (Na^+ and Ca^{2+}) increases up to 25% can be observed. No trend in terms of a difference between gouge and rim zones materials in this regard can be observed.

For the low concentration tracer elements studied in batch sorption experiments in this work (i.e. Rb^+, Sr^{2+}, Cs^+, Ba^{2+}) one can, however with a few exceptions, state that a net leaching of these elements are taking place during the experiment. Combining this with the fact that during the batch sorption experiment radiotracer elements are found to largely attach to the solid phase, it can be stated that there is an isotope exchange taking place between the solid and aqueous phase which explains the loss in the aqueous phase. It is clearly shown that the sorption do not occur as a general decrease of the total chemical concentration of the tracer element in the water phase.

The net leaching of tracer elements in combination with the strongly increased concentration of Al observed, indicates the possibility of chemical weathering (i.e. dissolution) taking place in the environments used for the batch experiments. Al was not introduced to the synthetic groundwater; the low concentration of ~3 ppb nevertheless measured in the blank samples of the synthetic groundwater, must be regarded as an effect of impurities in the salts introduced to that water. After 5 years of rock contact, the concentration has strongly increased; for a number of samples even up to several tenths of ppm. Such high concentrations are, to the knowledge of the authors, very uncommon for natural groundwaters and may be an indication that these batch sorption experiment environments give rise to chemical conditions that are not representative of natural groundwater conditions.

A plausible explanation for the high Al concentrations could be the existence of colloidal material originating from the rock material used in the experiment. However, the water samples have undergone strong centrifugation (3,000 G) followed by filtering through 20 nm filter. For comparative purposes, one sample was sampled without this filtration but showed, somewhat unexpectedly, higher Al concentrations than the corresponding sample that was filtered.

Nevertheless, for the purpose of simply studying a difference in the total ionic strength that may change the competitive force for the cation exchange sorption, the results indicate that the changes are comparatively small. Their potential for causing variations in cation exchange must be considered as small compared to the general uncertainty observed for the batch sorption experiment results.

Table 4-14. Changes (increase) in the water phase induced during batch sorption experiment. The reference is the measured concentration in the blank sample of prepared synthetic groundwater. This sample is compared to the concentrations aimed by the recipe of the synthetic groundwater (full agreement would be obtained without measurement uncertainties, adsorption on test tube walls and/or impurities in the chemicals used for the preparation) an is also compared to the measured concentration of the water that have been in contact with the different rock materials.

	Synthetic Groundwater, blank sample (mg/l)	Recipe	1596 m (NE-2)	KI0025F 194 m	1303 (NE-1)
Li	1.02	–13%	–41%	–9%	–5%
Na	2,120	–2%	13%	10%	28%
K	9.34	–14%	18%	380%	110%
Rb	0.0254	14%	52%	250%	420%
Cs	0.00474	–58%	110%	–38%	210%
Mg	42.5	1%	21%	36%	27%
Ca	1,500	–5%	14%	9%	32%
Sr	22	–11%	10%	3%	25%
Ba	0.0813	–27%	120%	131%	220%
Fe	0.004	2,400%	0%		
Mn	0.146	99%	84%	103%	55%
S	109	–1%	10%	10%	47%
Si	6.96	–31%	–67%	11%	–64%
Al	0.00358	not added	450%	420%	25,000%

	Synthetic Groundwater, blank sample (mg/l)	KI0023B 86 m #13	KI0023B 111 m #19	KI0025F 166 m #19 Filtered	KI0025F 166 m #19 Non-filtered	KI0023B 69 m #20	KI0025F02 74 m #20
Li	1.02	0%	1%	0%	–6%	–4%	9%
Na	2,120	12%	8%	17%	16%	5%	28%
K	9.34	32%	7%	18%	11%	6%	30%
Rb	0.0254	47%	18%	69%	61%	11%	110%
Cs	0.00474	43%	12%	35%	33%	–1%	230%
Mg	42.5	16%	10%	18%	14%	5%	29%
Ca	1,500	11%	5%	15%	13%	4%	26%
Sr	22	8%	3%	13%	11%	0%	23%
Ba	0.0813	60%	27%	49%	39%	41%	70%
Fe	0.004			43%	170%		780%
Mn	0.146	79%	16%	48%	42%	20%	51%
S	109	11%	5%	11%	12%	2%	22%
Si	6.96	–5%	–25%	–36%	–38%	–29%	–3%
Al	0.00358	1,100%	2,800%	20,000%	760%	860%	14,000%

5 Conclusions

5.1 Conclusions of the sorption and desorption experiments

The following conclusions can be summarized from the present work:

- The sorption coefficients determined in this work follow the relative order, i.e. $Na^{+}<Ca^{2+}\approx Sr^{2+}<Rb^{+}\approx Ba^{2+}<Cs^{+}$, observed in earlier laboratory investigations mainly focusing on non-altered rock material from the Äspö HRL (e.g. Byegård et al. 1998). In this work the Mn^{2+} and Ra^{2+} tracers have also been included, where the sorption of the Mn^{2+} tracer has been found to be, for the majority of the fault gouge materials studied, more strongly sorbing than e.g. Cs^{+}. The K_d for Ra^{2+} is for all cases studied (with one exception) highest in comparison with all other tracers studied.
- Fault gouge material has been identified as a strongly sorbing material; in most cases the K_d for these materials are found to be more than 1–2 order of magnitude higher than the corresponding rim zone material at the same sampling location. This is an indication that, at least for short term *in situ* experiment, the retention may very well be governed by the interaction with fault gouge material in direct contact with the flowing water in the studied flow path, e.g. as proposed by e.g. Andersson et al. (2004).
- There is a pronounced heterogeneity in the sorption for the fault gouge material as noticed from variable results on material from different locations in the same geological structure.
- Regarding the sorption of gouge material as a function of measured BET surface area (Figure 5-1), the correlation is rather poor. One can also observe that high sorption of one tracer does no necessary imply that high sorption of other tracers is to be expected; an observation which probably can be explained by the heterogeneity in the mineralogical composition of the materials (and structures) studied. For example:
  - The high BET surface area associated with material from KSH02 743 m contains hematite which is expected to promote surface complexation sorption. Accordingly, the sorption of Mn^{2+} is high, opposite to the cation exchange sorbing Cs^{+} which sorption is comparatively low, despite the high BET surface.
  - The KAS04 65 m (EW-1) material also has a high BET surface area, but the absence of e.g. hematite and presence of e.g. illite, mixed layer clay and kaolinite promotes cation exchange rather than surface complexation. Therefore the K_d of Cs^{+} is one order of magnitude higher than for Mn^{2+} in this case.

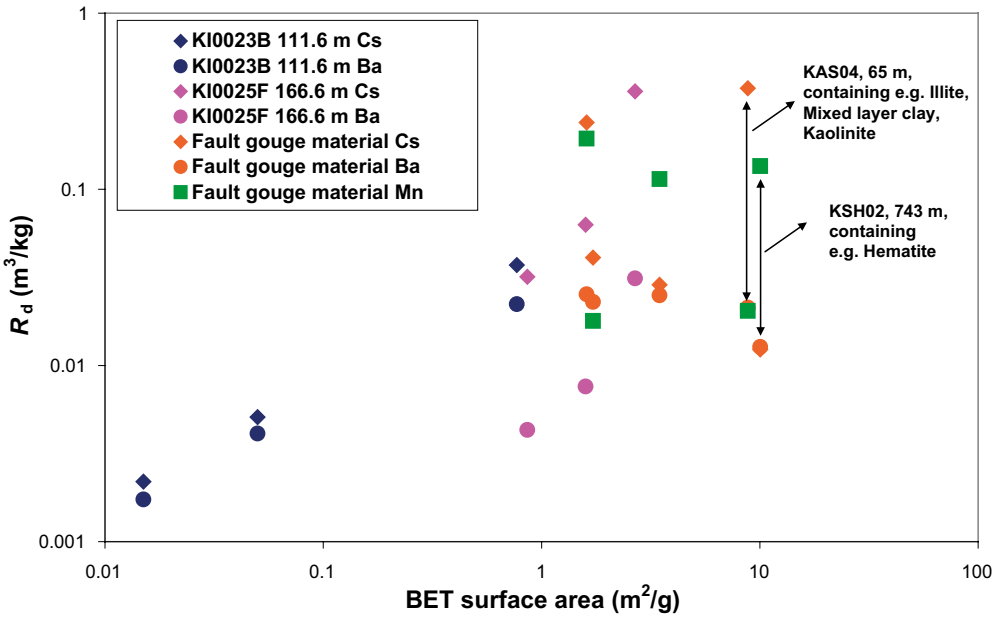

Figure 5-1. *Sorption distribution coefficients (R_d, m^3/kg) as a function of the measured BET surface area.*

- The technique used for studying the sorption of Ra^{2+}, i.e. a total concentration 5 µg/kg ($= 2 \cdot 10^{-10}$ M) and measurements using liquid scintillation counting with α-β discrimination with pulse shape analyses (PSA), worked out very well. This possibility of obtaining very low α background counting rate favor future use of α-emitting tracers in different sorption studies (laboratory and/or *in situ*). The present investigation shows that a large dynamic range can be obtained without having to use high concentrations, i.e. trivalent and tetravalent α-emitting should be possible to use in a sorption experiment and still be able to be far below the solubility limit of these elements.
- The solid phase measurements applied in the sorption studies for very weakly sorbing tracers, i.e. Na^{+}, indicate that earlier work may have underestimated the K_d.
- The concept of extrapolation of sorption results of different size fractions to a process consisting of a combination of outer surface sorption (K_a) together with inner surface sorption (K_d) has been tested. The extrapolation gives high uncertainties for the extrapolated K_d and for one case the extrapolation gives a negative value. Model calculations using the time dependence in the batch sorption experiment show poor conceptual agreement to an inner-outer surface model which therefore raises doubt in the validity of this sorption model.
- The desorption studies indicate that there is a considerable portion of the adsorbed tracers that are not desorbed using a strong electrolyte, i.e. 1 M NH_4Ac. Indications have been obtained suggesting that there are characteristics in the adsorption that can not be explained by a simple cation exchange mechanism.
- Concerning the Cation Exchange Capacity (CEC) determinations, it is indicated that the ISO 13536 method (saturation with Ba^{2+} followed by desorption with Mg^{2+}) is not sensitive enough for measurements of rock material. The newly established method ISO 23470 (saturation with Co-hexamine) gave results that were in agreement with the sorption results and is proposed as a method much more suitable for measurement of CEC for rock material.
- An alternative technique for determining K_d by comparison of leaching results (Co-hexamine leaching for cation exchange sorbing tracers, EDTA leaching for surface complexation sorbing tracers) has been tested and has been found promising.

5.2 Comparison with tabulated sorption coefficients

In Table 5-1, comparisons of the K_d obtained in this work are compared with values in the SKB generic sorption database (Carbol and Engkvist 1997) and also with the MIDS database used for modelling of the TRUE-1 *in situ* tracer experiments (Winberg et al. 2000). Values for intact unaltered Äspö rock are given for a saline groundwater environment.

As can be seen, the values reported for the rim zone material are lower than the values in the SKB generic database. The explanation for this is probably that the outer/inner surface extrapolation concept used in this investigation gives lower K_d; the same concept has not been applied in the work cited by Carbol and Engkvist (1997). The MIDS (Byegård et al. 1998) data set was evaluated from diffusion experiments and K_d–values are found to be in extreme lower interval of those values obtained on the basis of the current investigation of rim zone materials. However, K_d values evaluated from diffusion experiments have been suspected to be underestimated due to the impact of micro-scale heterogeneity in the porosity distribution, cf. e.g. Byegård et al. (2001). It should, however, also in this context be referred to the discussion in this report of uncertainty involved in the inner/outer surface evaluation concept, cf. Section 4.2.1. This evaluation uncertainty could provide an explanation for the large spread in the K_d obtained for the rim zone material.

The K_d-values obtained for the fault gouge material are significantly higher than the corresponding values for the rim zone material at the same locality and are thus also comparable to the MIDS values. Based on the mineralogy and the large surface areas of this material, the high K_d-values are not unexpected. The observation that the values of generic database for granitic rock are more close to the values for the fine-grained fault gouge material than to the rim zone material (at least for Sr^{2+} and Cs^{+}) is considered not satisfactory and calls for a general review of the sorption database.

A possible explanation for the deviation could be that different contact times have been applied in the experiments of this work compared to those of the referred work in the literature review by Carbol and Engkvist (1997). This explanation is difficult to verify since the authors of the review do not address the aspect of contact times, or the aspect of diffusion onto inner surfaces, in their method for selecting data.

Table 5-1. K_d for Sr^{2+}, Cs^+ and Ra^{2+} determined in this study compared with corresponding values earlier used for interpretation of *in situ* experiments (Byegård et al. 1998) and the database used for performance assessment purposes (Carbol and Engkvist 1997).

Investigation	Method/evaluation	K_d (m^3/kg)		
		Sr^{2+}	Cs^+	Ra^{2+}
Rim zone material, TRUE Block Scale (this work), min-max values	Batch sorption experiment, outer/inner surface evaluation from 3 different size fractions of crushed rock material	2.0E–6 – 1.4E–4	< 5E–4 – 1.2E–2	–
	Batch sorption experiment, 1–2 mm size fraction	3.4E–5 – 2.2E–4	2.1E–3 – 3.2E–2	1.3E–2 – 3.1E–2
Fault gouge material, Äspö Hard Rock Laboratory (this work), min-max values	Tracer distribution coefficient measured on the <0.125 mm size fraction of loose fracture material	6.1E–4 – 2.0E–3	1.2E–2 – 3.7E–1	3.6E–1 – >1.3E+0
MIDS (Byegård et al. 1998)	Evaluation from retardation in diffusion experiments using intact Äspö diorite	4.7E–6	8E–4	–
SKB generic database (Carbol and Engkvist 1997, min-max values)	Selection from a literature review on sorption data from studies using granitic material	(1–10)E–4	(1–10)E–2	(1–10)E–2

References

SKB's (Svensk Kärnbränslehantering AB) publications can be found at www.skb.se/publications.

Andersson P, Byegård J, Dershowitz, B, Doe T, Hermanson J, Meier P, Tullborg E-L, Winberg A, 2002a. Final report of the TRUE Block Scale project. 1. Characterisation and model development. SKB TR-02-13, Svensk Kärnbränslehantering AB.

Andersson P, Byegård J, Winberg A, 2002b. Final report of the TRUE Block Scale project. 2. Tracer tests in the block scale. SKB TR-02-14, Svensk Kärnbränslehantering AB.

Andersson P, Byegård J, Tullborg E-L, Doe T, Hermanson J, Winberg A, 2004. In situ tracer tests to determine retention properties of a block scale fracture network in granitic rock at the Äspö Hard Rock Laboratory, Sweden. Journal of Contaminant Hydrology 70, 271–297.

Andersson P, Byegård J, Billaux D, Cvetkovic V, Dershowitz W, Doe T, Hermanson J, Poteri A, Tullborg E-L, Winberg A, 2007. TRUE Block Scale Continuation project. Final report. SKB TR-06-42, Svensk Kärnbränslehantering AB.

Bruggenwert M G M, Kamphorst A, 1982. Survey of experimental information on cation exchange in soil systems. In Bolt G H (ed). Soil chemistry. B, Physico-chemical models. Amsterdam: Elsevier, 141–203.

Byegård J, Skarnemark G, Skålberg M, 1995. The use of some ion-exchange sorbing tracer cations in in situ experiments in high saline groundwaters. In Murakami T, Ewing R C (eds). Scientific basis for nuclear waste management XVIII: symposium held in Kyoto, Japan, 23–27 October 1994. Pittsburgh, PA: Materials Research Society. (Materials Research Society Symposium Proceedings 353), 1077–1084.

Byegård J, Johansson H, Skålberg M, Tullborg E-L, 1998. The interaction of sorbing and non-sorbing tracers with different Äspö rock types. Sorption and diffusion experiments in the laboratory scale. SKB TR-98-18, Svensk Kärnbränslehantering AB.

Byegård J, Widestrand H, Skålberg M, Tullborg E-L, Siitari-Kauppi M, 2001. First TRUE Stage. Complementary investigation of diffusivity, porosity and sorptivity of Feature A-site specific geologic material. SKB ICR-01-04, Svensk Kärnbränslehantering AB.

Byegård J, Ramebäck H, Widestrand H, 2002. Äspö Hard Rock Laboratory. TRUE-1 Continuation project. Use of radon concentrations for estimation of fracture apertures – Part 1: Some method developments, preliminary measurements and laboratory experiments. SKB IPR-02-68, Svensk Kärnbränslehantering AB.

Byegård J, Selnert E, Tullborg E-L, 2008. Bedrock transport properties; Data evaluation and retardation model. Site descriptive modeling, SDM-Site Forsmark. SKB R-08-98, Svensk Kärnbränslehantering AB.

Carbol P, Engkvist I, 1997. Compilation of radionuclide sorption coefficients for performance assessment. SKB R-97-13, Svensk Kärnbränslehantering AB.

Comans R N J, Hockley D E, 1992. Kinetics of cesium sorption on illite. Geochimica et Cosmochimica Acta 56, 1157–1164.

Comans R N J, Haler M, De Preter P, 1991. Sorption of cesium on illite: non-equilibrium behavior and reversibility. Geochimica et Cosmochimica Acta 55, 433–440.

Dershowitz W, Winberg A, Hermanson J, Byegård J, Tullborg E-L, Andersson P, Mazurek M, 2003. Äspö Hard Rock Laboratory, Äspö Task Force on modeling of groundwater flow and transport of solutes. Task 6c. A semi-synthetic model of block scale conductive structures at the Äspö HRL. SKB IPR-03-13, Svensk Kärnbränslehantering AB.

Gunnarsson M, Jakobsson A-M, Ekberg S, Albinsson Y, Ahlberg E, 2000. Sorption studies of cobalt(II) on colloidal hematite using potentiometry and radioactive tracer technique. Journal of Colloid and Interface Science 231, 326–336.

Hakami E, Wang W, 2005. Äspö Hard Rock Laboratory. TRUE-1 Continuation project. Fault rock zones characterisation. Characterisation and quantification of resin-impregnated fault rock pore space using image analysis. SKB IPR-05-40, Svensk Kärnbränslehantering AB.

Hermanson J, Doe T, 2000. Äspö Hard Rock Laboratory. TRUE Block Scale project. Tracer test stage. March'00 structural and hydraulic model based on borehole data from KI0025F03. SKB IPR-00-34, Svensk Kärnbränslehantering AB.

Marmier N, Delisée A, Fromage F, 1999. Surface complexation modeling of Yb(III), Ni(II), and Cs(I) sorption on magnetite. Journal of Colloid and Interface Science 211, 54–60.

Poteri A, Billaux D, Dershowitz W, Gómez-Hernández J J, Cvetkovic V, Hautojärvi A, Holton D, Medina A, Winberg A (ed), 2002. Final report of the TRUE Block Scale project. 3. Modeling of flow and transport. SKB TR-02-15, Svensk Kärnbränslehantering AB.

Rose A W, Bianchi-Mosquera G C, 1993. Adsorption of Cu, Pb, Zn, Co, Ni, and Ag on goethite and hematite; a control on metal mobilization from red beds into stratiform copper deposits. Economic Geology 88, 1226–1236.

Selnert E, Byegård J, Widestrand H, Carlsten S, Döse C, Tullborg E-L, 2009. Bedrock transport properties; Data evaluation and retardation model. Site descriptive modeling, SDM-Site Laxemar. SKB R-08-100, Svensk Kärnbränslehantering AB.

Widestrand H, Byegård J, Ohlsson Y, Tullborg E-L, 2003. Strategy for the use of laboratory methods in the site investigations programme for the transport properties of the rock. SKB R-03-20, Svensk Kärnbränslehantering AB.

Winberg A, Andersson P, Hermanson J, Byegård J, Cvetkovic V, Birgersson, L, 2000. Äspö Hard Rock Laboratory. Final report of the first stage of the tracer retention understanding experiments. SKB TR-00-07, Svensk Kärnbränslehantering AB.

Appendix A

Results of the chemical analyses of the rock material

	Gouge material, sampled, <0.125 mm size fraction				Rim zone material, crushed and sieved					
					KI0023B 111 m , size fraction (mm)			KI0025F 166 m, size fraction (mm)		
Element	1596 m (NE-2-Zone)	KI0025F 194 m	1303-NE-1	KAS 04:65 m EW-1	<0.125	0.25–0.5	1–2	<0.125	0.25–0.5	1–2
SiO_2 (%)	32.3	71.4	70.6	58.5	54.1	57.3	58.5	53.4	55.8	56.1
Al_2O_3	15.1	13.0	12.7	20.6	17.1	17.8	17.9	17	17.7	18
CaO	2.96	1.27	1.12	0.427	7.67	7.25	6.92	7.28	7.16	7.49
Fe_2O_3	16.8	3.31	4.54	2.69	9.12	6.28	5.89	9.6	7.42	7.03
K_2O	1.12	6.63	6.07	11.9	1.95	1.9	1.78	2.42	2.33	2.2
MgO	18.9	0.899	1.88	1.54	2.39	1.86	1.67	2.64	2	1.63
MnO	0.345	0.0401	0.0686	0.0295	0.115	0.0899	0.0841	0.155	0.127	0.118
Na_2O	0.228	2.44	0.136	0.125	4.05	4.71	4.91	3.38	4.14	4.42
P_2O_5	0.302	0.142	0.109	0.116	0.396	0.386	0.407	0.375	0.29	0.33
TiO_2	1.05	0.395	0.266	0.595	0.911	0.924	0.94	0.767	0.758	0.79
Summa	89.1	99.5	97.5	96.5	97.8	98.5	99	97	97.7	98.1
LOI	8.9	0.3	3.0	3.3	2.2	2.1	1.5	3.5	2.1	2.1
Ba (mg/kg)	152	1,040	1,360	114.50	984	1,010	952	737	815	821
Be	6.49	1.69	8.41	12.4	2.38	2.55	2.4	4.66	3.79	3.35
Co	72.3	<6	<6	<6	26.9	13.1	11.5	19.1	9.83	8.22
Cr	1,700	18.4	14.0	<10	1,920	216	55.2	1,240	125	41.7
Cs	2.25				0.687	0.567	0.515	4.74	3.11	2.26
Cu	26.9	201	226	483	13.8	8.01	<6	24.9	<6	<6
Ga	27.3	45.9	58.3	74.4	21.8	22.4	21.5	24.5	24	24.9
Hf	3.64	6.69	2.50	10.9	6.64	6.53	6.63	6.76	4.36	5.57
Mo	<2	66.4	6.85	5.19	64.9	7.37	<2	63.4	3.72	<2
Nb	9.26	16.6	7.37	42.4	16.9	15.3	14.4	13.4	12.1	12.2
Ni	505	<10	13.1	<10	70.6	29.1	25.3	59.8	24.1	21
Rb	50.2	166	215	490	65.4	55.8	55.1	84.3	68.1	60.1
S	139				866	255	340	345	161	50.4
Sc	33.6	2.09	4.15	4.05	10.9	11.5	11.7	10.2	10.4	10.9
Sn	7.14	2.68	9.88	21.8	5.73	3.24	3.07	6.72	2.69	2.46
Sr	139	184	293	81.4	2,150	2,210	2,200	1,830	2,060	2,180
Ta	0.785	0.557	0.500	3.04	0.961	0.971	1.07	0.73	0.763	0.763
Th	7.41	30.4	6.43	14.9	5.65	5.32	5.36	4.64	4.65	3.88
U	4.32	5.74	7.34	12.4	2.65	2.58	2.54	2.73	2.78	2.5
V	209	41.8	109	22.5	188	123	115	185	135	127
W	3.03	158	2.30	4.13	98	9.68	1.5	64.1	7.02	2.08
Y	19.9	24.6	8.70	45.2	20.6	27.2	27.3	27	31.1	33.5
Zn	545	71.8	142	158	130	86.8	60.3	218	141	121
Zr	131	396	92.7	563	282	303	307	334	211	251
La	17.5	32.8	23.9	16.3	56.9	55.4	56	60.5	59.9	62.7
Ce	36.7	73.3	48.6	30.7	119	122	118	123	124	132
Pr	3.77	9.01	6.27	4.41	14.4	14.3	14.1	15	15.3	15.6
Nd	14.6	32.5	21.6	15.9	52.5	54.5	52.6	55.2	57.8	59.5
Sm	3.21	9.96	7.51	7.16	8.23	8.62	8.79	9.58	10.1	10.4
Eu	0.666	1.23	0.637	0.605	2.14	2.19	2.26	2.21	2.33	2.52
Gd	3.67	5.97	2.61	3.46	6.04	5.68	5.63	7.44	7.64	8.03
Tb	0.64	0.860	0.424	0.780	0.75	0.737	0.717	0.923	0.919	1.02
Dy	4.22	4.54	2.26	6.11	4.33	4.17	4.35	5.09	4.76	5.2
Ho	0.803	0.947	0.504	1.71	0.744	0.748	0.766	0.931	0.891	0.966
Er	2.41	8.72	5.88	11.5	2.15	2.14	2.13	2.54	2.39	2.5
Tm	0.308	1.24	0.896	2.02	0.307	0.294	0.312	0.33	0.305	0.315
Yb	2.07	2.31	1.37	7.63	1.97	1.97	2.02	2.21	1.99	2.2
Lu	0.223	0.474	0.331	1.27	0.269	0.24	0.25	0.311	0.239	0.248